Quaternary Science Reviews 344 (2024) 109005

Contents lists available at ScienceDirect

Quaternary Science Reviews

journal homepage: www.elsevier.com/locate/quascirev

Sedimentary response of the Po Basin to Mid-Late Pleistocene glacio-eustatic oscillations

Luigi Bruno [a,*], Luca Demurtas [a], Donatella Magri [b], Fabrizio Michelangeli [b], Tammy Rittenour [c], Wan Hong [d], Veronica Rossi [e], Stefano Claudio Vaiani [e], Amanda Vecchi [e], Alessandro Amorosi [e]

[a] Department of Chemical and Geological Sciences, University of Modena and Reggio Emilia, Via Campi 103, 41125, Modena, Italy
[b] Department of Environmental Biology, Sapienza University of Rome, Piazzale Aldo Moro 5, 00185, Roma, Italy
[c] Luminescence Lab, Utah State University, 1770 North Research Parkway Suite 123, North Logan, UT, 84341, United States
[d] KIGAM Korea Institute of Geoscience and Mineral Resources, 92 Gwahangro, Yuseong-gu, Daejeon Metropolitan City, South Korea
[e] Department of Biological, Geological and Environmental Sciences, University of Bologna, Via Zamboni 67, 40125, Bologna, Italy

ARTICLE INFO

Handling editor: Giovanni Zanchetta

Keywords:
Coastal system
Sediment supply
Core stratigraphy
Po plain
Quaternary

ABSTRACT

The Middle and Late Pleistocene were characterized by high-amplitude climate and sea-level oscillations that deeply influenced the evolution of alluvial and coastal systems worldwide. Through the correlation of 43 cores and 168 well data, with the aid of pollen, meiofauna, ^{14}C, ESR and IRSL data, this work provides a detailed reconstruction of the Middle Pleistocene to Holocene stratigraphy of the Po Basin and explores the sedimentary response of the Po-Adriatic alluvial-coastal system to glacio-eustatic oscillations and other concomitant forcing factors.

The Middle Pleistocene to Holocene sedimentary succession of the Po Basin is composed of alluvial, paralic, coastal and shallow-marine facies associations arranged in an overall shallowing-upward trend. This general trend is punctuated by the rhythmical alternation of progradationally stacked coastal wedges with thick alluvial deposits. At landward locations, where the coastal facies wedge out, the depositional cyclicity records alternating paralic and alluvial facies associations. The overall shallowing-upward trend documents the longer-term, progressive filling of the basin driven by high sediment supply which overcame the rate of creation of accommodation induced by subsidence. The cyclic arrangement of facies, paralleled by rhythmical changes in vegetation, reflects Milankovitch-scale, glacio-eustatic oscillations in the 100 ka band. Increasing subsidence towards the sea and the activity of selected sectors of the buried Apennine thrust front, might have enhanced the seaward migration of coastal wedges.

This study provides clues on the sedimentary response of a low-gradient coastal system to dramatic climatic and eustatic changes. The model of basin evolution presented here may help predict the environmental modifications of coastal areas in near future scenarios of climate and sea-level change.

1. Introduction

The Middle and Late Pleistocene are marked by high-amplitude climate and sea-level oscillations linked to periodic variations in the Earth's orbital parameters (Lisiecki and Raymo, 2005). Eight glacial cycles with period of ca. 100 ka resulted in eustatic oscillations of ca. 100 m (Rohling et al., 2009, 2013, 2014; Grant et al., 2014). Sedimentary systems worldwide responded to these perturbations, recording distinctive cyclic lithofacies patterns. The rhythmical occurrence of siliciclastic clays in marine carbonate successions (Bacon, 1984; Thomson et al., 1999), ice-rafted detritus in polar-regions shelf successions (Henrich et al., 1989; Larter and Cunningham, 1993), paleosols in aeolian-loess deposits (Nielsen et al., 2004; Marković et al., 2007; Obreht et al., 2016), till and glacio-fluvial deposits alternating with alluvial sediments in periglacial settings (Marks et al., 2019), are just few examples of depositional cyclicity reported from the Middle Pleistocene sedimentary record. Terrestrial records also include lacustrine successions, where the glacial-interglacial signal can be read in cyclic changes in pollen assemblages (Follieri et al., 1988; Tzedakis et al., 1997; Camuera et al., 2019). However, as lakes are typically disconnected by

* Corresponding author.
E-mail address: luigi.bruno@unimore.it (L. Bruno).

https://doi.org/10.1016/j.quascirev.2024.109005
Received 11 June 2024; Received in revised form 10 October 2024; Accepted 11 October 2024
Available online 19 October 2024

the sea, lacustrine sequences provide poor information about how eustatic changes affected sedimentation. Coastal areas, instead, are particularly sensitive to sea-level changes and provide an effective record of Mid-Late Pleistocene glacio-eustatic oscillations. Worldwide continental shelves were exposed during falling stages and sea-level lowstands, and then submerged during marine transgressions and highstands, with hundreds-km facies shifts along low-gradient shelves (Liu et al., 2003; Storms et al., 2008; Blum et al., 2013; Yao et al., 2020; Thanh et al., 2021). River systems responded to eustatic drops excavating deep valleys, which were filled with estuarine sediments during the following phases of sea-level rise (Allen and Posamentier, 1993; Blum and Aslan, 2006; Chaumillon et al., 2008; Vis and Kasse, 2009; Tanabe et al., 2015; Peeters et al., 2016; Rossi et al., 2017; Gao et al., 2022). Thus, climatic and sea-level oscillations introduce an oscillatory signal in the geological record of sedimentary basins, through the alternation of continental and paralic or shallow-marine deposits. Similar cyclothemes have also been observed in ancient sedimentary succession, generally superposed to an overall shallowing-upward trend (Bentham et al., 1992; Krapez, 1996; Changsong et al., 2004; Yang, 2011; Fielding, 2021; Liu et al., 2023). Most of the Quaternary studies exploring the sedimentary response of coastal and alluvial systems to glacio-eustatic changes are limited to the transition from the Last Glacial Maximum lowstand to the present-interglacial highstand, because of the temporal range of ^{14}C (last 50 ka), (Blum, 2007; Xu et al., 2016). The recent development of dating methods beyond the ^{14}C window (e.g. luminescence, cosmogenic nuclides) has led to the progressive increase of chronologically constrained stratigraphic studies encompassing the entire Late Pleistocene (Busschers et al., 2005; Thanh et al., 2021). By contrast, few studies have explored the sedimentary response of alluvial-coastal systems to the Middle Pleistocene climate and eustatic forcing (Carter and Naish, 1998; Sun et al., 2022). Several works on Middle-Pleistocene stratigraphy rely upon the detailed study of outcrops from exhumed successions (e.g. Rose, 2009; Marks et al., 2019). In these settings, stratigraphic correlations are hindered by differential tectonic uplift, abundance of depositional hiatuses and large distance between representative outcrops (Rose, 2009). On the contrary, in subsiding basins, sedimentary units and their stratigraphic relationships are better preserved, and stratigraphic correlations can be more effective, especially if supported by detailed facies analysis and by a good coverage of core, well log, and seismic data (Cui et al., 2008; Hollis et al., 2019).

The Po-Adriatic basin is a subsiding foreland basin, that has been the object of several stratigraphic studies in the last decades (e.g. Amorosi et al., 2004; Ghielmi et al., 2013). The effects of Middle and Late Pleistocene glaciations (and related eustatic changes) on sedimentation patterns in the Po-Adriatic Basin have been documented in a vast literature. A cyclic organization of facies has been reported for the fully alluvial portion of the basin (Amorosi et al., 2001, 2008) and for the coastal plain (Amorosi et al., 2004; Massari et al., 2004; Marcolla et al., 2021; Rossi et al., 2021). These works were limited to relatively small areas and did not produce a comprehensive stratigraphic and evolutionary picture of the Po-Adriatic Basin. An exception is the work by Campo et al. (2020), who built a general model of Upper Pleistocene to Holocene stratigraphy from the alluvial to the coastal realms and provided a detailed paleogeographic reconstruction of the Po coastal plain during MIS 5e, constrained by ESR ages (see Ferranti et al., 2006).

In general, the lack of basin-scale studies on the Middle Pleistocene stratigraphy of the Po Basin is attributable to: (i) the poor resolution of industrial seismic profiles in this stratigraphic interval; (ii) the relatively low number of cores penetrating Middle Pleistocene units, which are typically encountered at depths >100 m; (iii) the increasing tectonic deformation with depth, which makes stratigraphic correlation uncertain, especially close to the buried tectonic structures (Amorosi et al., 2021); (iv) the lack of absolute ages. In fact, the chronology of Middle Pleistocene deposits, in the subsurface of the Po Basin, relied uniquely on pollen (Amorosi et al., 1999, 2008) and magnetostratigraphic (Muttoni et al., 2003, 2011) data. Gunderson et al. (2014) provided a detailed chronology of Middle Pleistocene deposits exposed at the basin margin, based on the integration of several dating methods. The dated succession, however, was strongly affected by local tectonics and is rather discontinuous. Similar limitations affect several other regions worldwide. A rare example of high-resolution investigation of Middle Pleistocene deposits is the one from the Rhine-Meuse system, which is based on a robust, OSL-based chronology (Busschers et al., 2005; Peeters et al., 2016). However, owing to a markedly lower subsidence, Middle Pleistocene deposits in this case were encountered at significantly lower depths.

In this work, we reconstructed the sedimentary evolution of the Po Basin since the Middle Pleistocene and examined the interaction between high-amplitude climate and sea-level oscillations and the progressive filling of the basin in shaping the Po-Adriatic paleogeography. To this aim, we reconstructed the subsurface stratigraphy through correlation of 43 core data and 6 pollen profiles along two stratigraphic cross-sections, 109 and 67 km long, respectively (Fig. 1). The absolute chronology was based on IRSL, ESR and ^{14}C dates. The resulting depositional architecture represents the first chronologically constrained reconstruction of high-resolution Middle and Late Pleistocene stratigraphy in the area.

2. Geological setting

The Po Basin represents the foredeep, filled with Plio-Quaternary sediments from the Northern Apennines and of the Southern Alps (Fig. 1). These two mountain belts, showing opposite vergence, developed since the Cretaceous due to the convergence between the European and Adria plates (Carminati and Doglioni, 2012). The most external portion of the two accretionary wedges is buried beneath the Po Plain and is composed of arcuate systems of thrust-related folds (Fantoni and Franciosi, 2010; Turrini et al., 2014). The Apennine Ferrara folds, tectonically active since the Early Pliocene (Toscani et al., 2009; Boccaletti et al., 2011; DISS Working Group, 2018), include the Mirandola thrust system which was active during the 2012 Emilia earthquake (Bonini et al., 2014). Atop the buried anticlines, the Po Basin fill is a few hundred meters thick, whereas in the depocenters it may attain 6–8 km (Fig. 2, Amadori et al., 2018).

The Po Basin fill has been subdivided on a seismic basis into six tectonically driven stratigraphic units (PL1s, PL2s, PL3s, PS1s, PS2s, PS3s, Ghielmi et al., 2013) bounded at their base by six unconformities (PL1, PL2, PL3, PS1, PS2, PS3 in Fig. 2). Units PL1s to PS2s are deep-water turbidites, whereas unit PS3s records the rapid progradation of the Po delta system, when sediment supply overcame the rate of creation of accommodation space; genetically related turbidites were deposited in the Northern Adriatic Sea (Amadori et al., 2020).

The alluvial units of the Po Basin (Po Supersynthem of Amorosi et al., 2008) constitute the upper portion of unit PS3s and are dated to the last 870 ka (Muttoni et al., 2003; Gunderson et al., 2014). The Po Supersynthem, poorly resolved in industrial seismic sections (Fig. 2), has been investigated through sedimentological, paleontological and palynological analyses on core sediments, which showed a cyclic organization of facies. At the basin margin, mud-prone overbank deposits alternate with fluvial-channel gravel and subordinate sand bodies (Fig. 3A, Gunderson et al., 2014). Here, the gravel-mud ratio increases around MIS11 (Fig. 3A, I and 4A; Garzanti et al., 2011; Muttoni et al., 2011; Gunderson et al., 2014).

In the central Po Plain, beneath the Po River, mud-dominated horizons alternate with sand bodies deposited by the Po River and by its alpine tributaries during glacial periods (Fig. 3D–G; Amorosi et al., 2008; Bruno et al., 2021; Demurtas et al., 2024). Mud-prone horizons host pollen typical of interglacial periods (broad-leaved trees), whereas pollen occasionally preserved within predominantly gravel and sand bodies indicates cold-climate associations (*Pinus*, mountain trees and herbs, Fig. 3F, G, 3H, Amorosi et al., 2008; see also Amorosi et al., 2001). The attribution of laterally continuous, coarse-grained sediment bodies

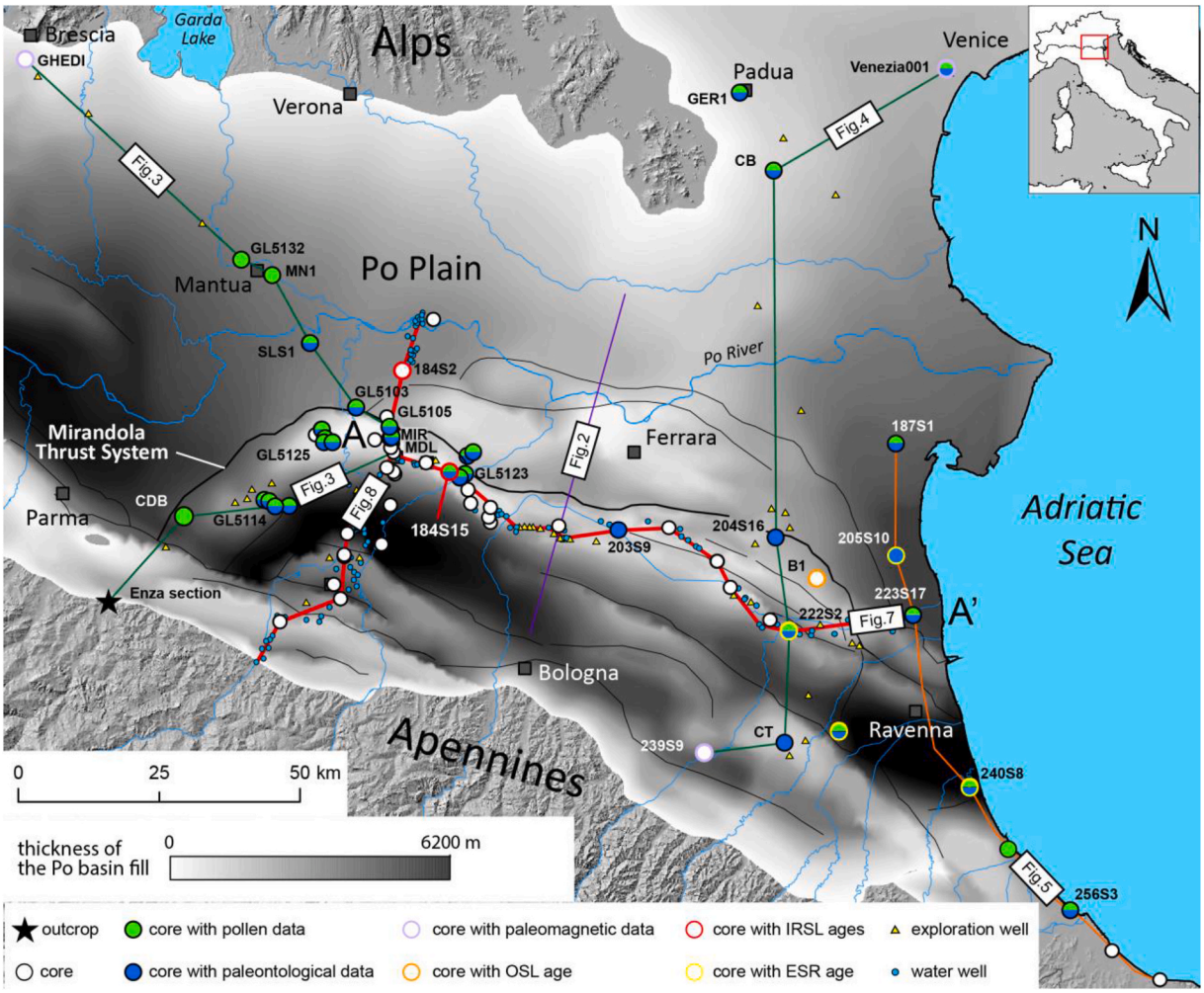

Fig. 1. The Po Basin with location of the stratigraphic sections of Figs. 2–5 and 8 and 9 and of cores and wells that compose the stratigraphic dataset. The thickness of the Po Basin fill is modified after Boccaletti et al. (2011).

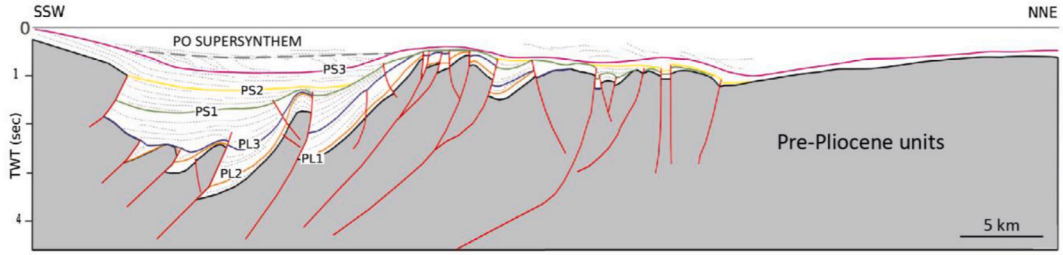

Fig. 2. Interpretation of a S-N oriented seismic profile with indication of the main angular unconformities within the Po Basin fill (modified after Amadori et al., 2019). See Fig. 1 for location.

to glacial periods is supported by OSL dates from the Enza River section (Gunderson et al., 2014, Fig. 3A).

In cores recovered close the Adriatic coastline, alluvial sediments deposited during glacial periods alternate with paralic, coastal and shallow-marine sediments deposited during the interglacials (Fig. 4C–G; Amorosi et al., 2004; Massari et al., 2004; Marcolla et al., 2021; Rossi et al., 2021). Coastal sediments assigned to MISs 5e and MIS 1, studied in detail by Amorosi et al. (2017) and Campo et al. (2020, Fig. 5), are arranged in transgressive-regressive wedges, with a markedly retrogradational stacking pattern of facies (transgressive systems tract, Bruno et al., 2017) overlain by a well-developed progradational parasequence set (highstand systems tract; Amorosi et al., 2020). The maximum landward position of the Adriatic coastline during MIS 1 and MIS 5e was about 25 and 35 km inland of the modern coastline (Bruno et al., 2017; Campo et al., 2020), respectively.

3. Methods

3.1. Stratigraphic dataset

In this work, the Middle-Late Pleistocene to Holocene stratigraphy of the central and eastern Po Plain was investigated over an area of ~3500 km^2 based on the correlation of 43 cores, 15–220 m long (Fig. 1). Two cores (184S2 and 184S15), recently recovered for the realization of

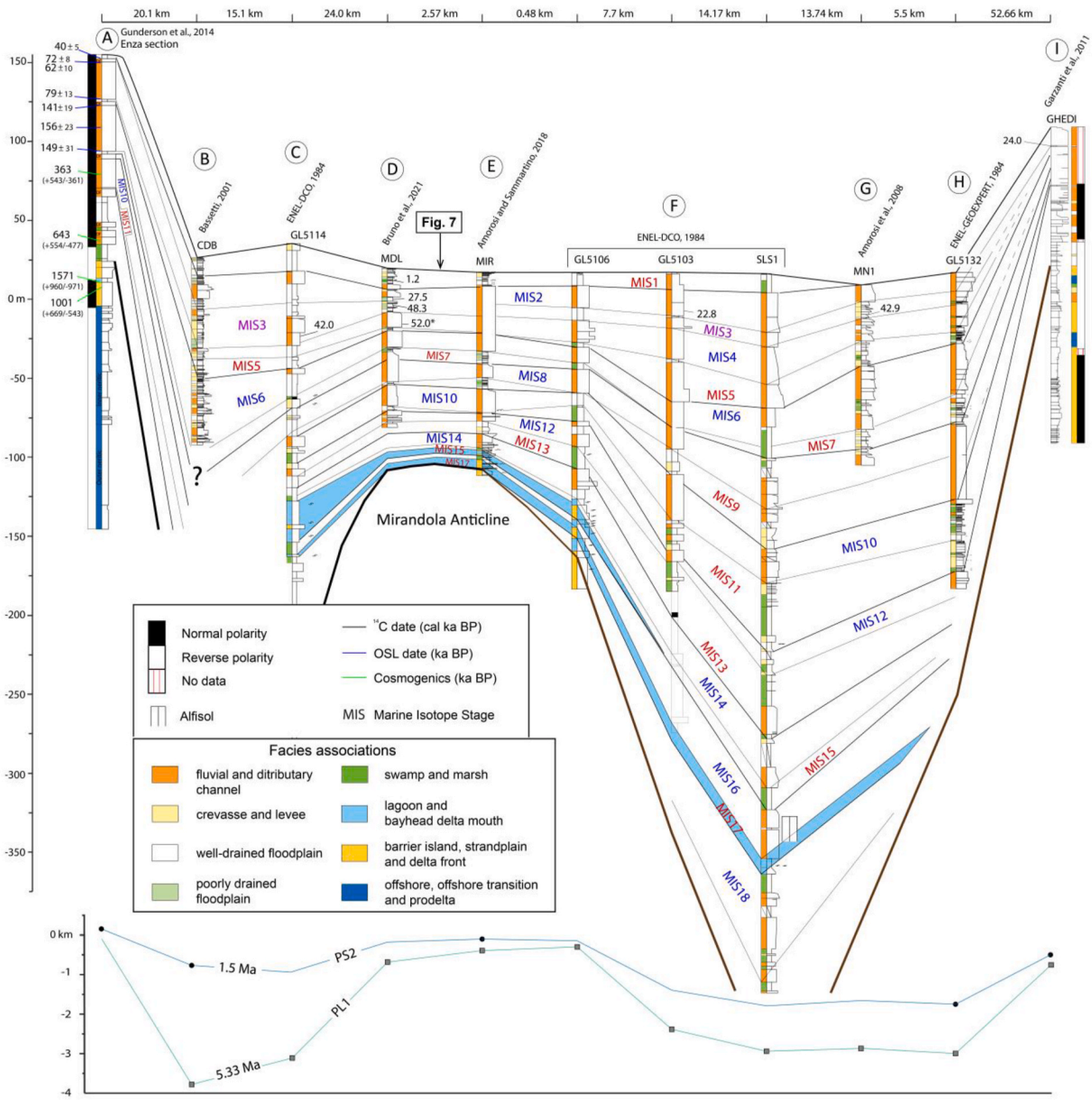

Fig. 3. – Stratigraphic correlation of cores from previous works which penetrated Middle and Late Pleistocene units of the inner Po Basin (see Fig. 1 for location). Unconformities PL1 and PS2 are from Boccaletti et al. (2011) and Amadori et al. (2019).

Sheet 184 of the Geological Map of Italy at 1:50,000 scale (GMI), were used as a reference for facies analysis. They were described reporting: grain size, grain size trends, color, consistency, and accessory components, such as plant remains, peat horizons, carbonate nodules, and shell fragments. Core 184S15 (176 m long) was selected for micropaleontological quantitative analyses, including pollen (section 3.3) and meiofauna (section 3.4). Thirty-eight core descriptions from published works (Amorosi et al., 1999; ENEL-DCO, 1984; Bruno et al., 2021; Demurtas et al., 2022, 2024; sheets 201, 202, 203, 204, 219, 222 and 223 of GMI), and from the Emilia-Romagna Geological, Soil and Seismic Survey database, were reinterpreted in terms of depositional facies associations, locally supported by published meiofauna and palynological data, and correlated into two stratigraphic sections. Section A-A′, 215 m deep, is elongated from land (WNW) to sea (ESE) for 109 km, along the Mirandola thrust system and its eastward prolongation (Fig. 1). Section B-B′, 250 m deep, runs transversal to the main tectonic structures, from the Apennine margin (SSW) to the Po River (NNE), ~100 km inland of the Adriatic coast. A total of 132 water wells and 36 exploration wells were also projected in the stratigraphic sections. Water wells (depth 30–700 m) provide low-resolution data on grain size and color, with local indication of fossils and peat, and were mainly used to reconstruct the geometry and lateral extent of sand bodies. Exploration wells, which report paleontological data and information about older stratigraphic surfaces, helped to trace the base of the Po Supersynthem and to reconstruct the geometry of the buried anticlines. Well logs were projected within a distance of 3 km. In areas of intense tectonic deformation, core data were projected from a maximum distance of 1 km and following the trend of the buried thrusts and folds.

Stratigraphic correlations were based on facies relationships, the lateral tracking of stratigraphic markers (e.g. paleosols, peat horizons), and pollen data. Absolute ages from 53 radiocarbon dates (18 from this work and 35 from ENEL-DCO, 1984; Bruno et al., 2021; Amorosi et al., 2021; Demurtas et al., 2022 and from the Sheets 202, 203, 222, 223 of GMI), 3 ESR dates (Ferranti et al., 2006) and 3 new IRSL ages (see section 3.2 for details) supported and validated stratigraphic correlations.

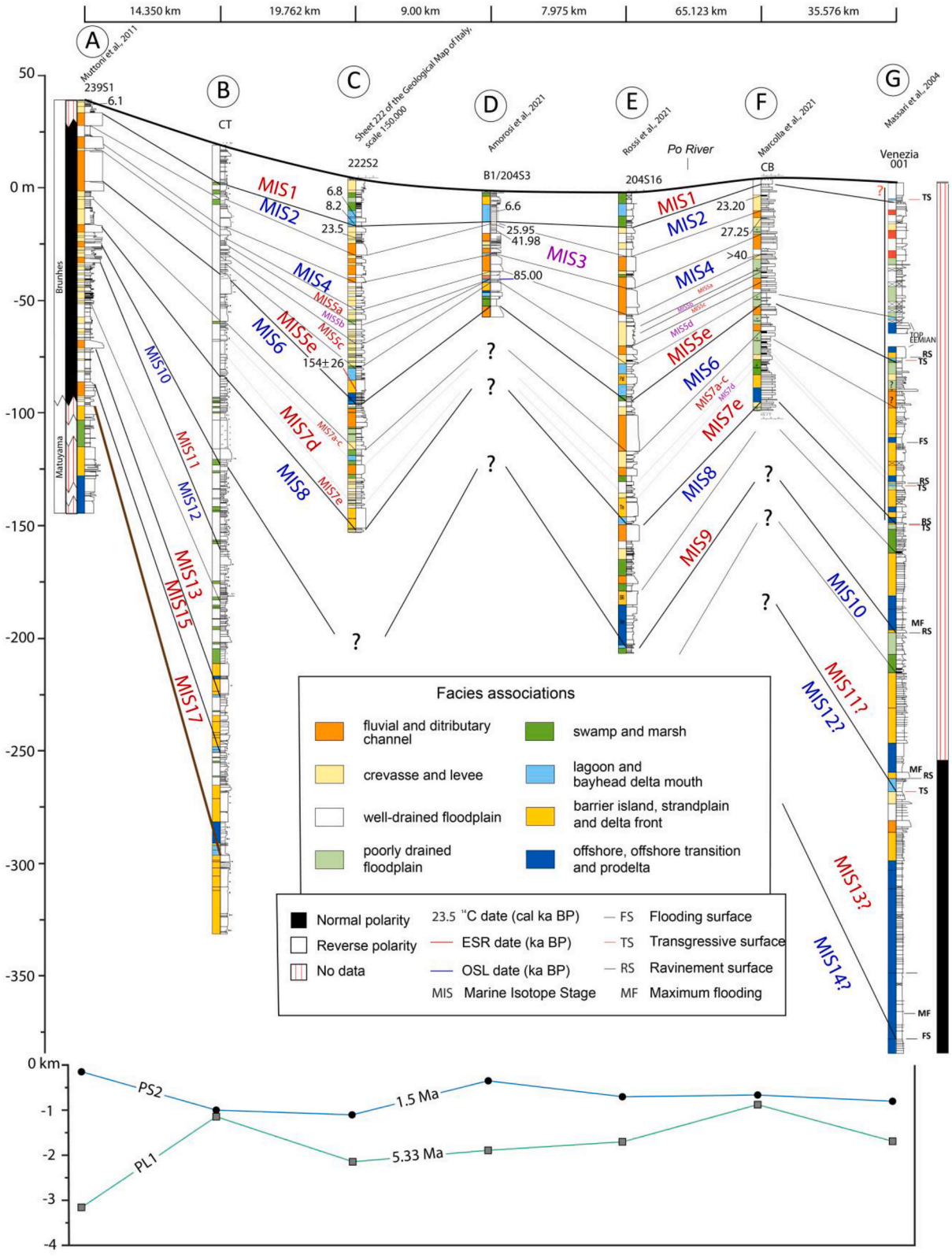

Fig. 4. Stratigraphic correlation of cores from previous works which penetrated Middle and Late Pleistocene units of the Po coastal plain (see Fig. 1 for location). Unconformities PL1 and PS2 are from Boccaletti et al. (2011) and Amadori et al. (2019).

3.2. Absolute chronology

Fifteen wood and soil samples were collected from cores 184S2, 184S5, 184S9, 184S13 and 184S15 (see Table 1) and ^{14}C-dated at the KIGAM Laboratory (Korea Institute of Geoscience and Mineral Resources, Daejeon, Republic of Korea). All samples were cleaned through acid-alkali-acid pretreatment, to remove secondary calcite and humic acids. Radiocarbon ages were calibrated using OxCal 4.4 (Bronk Ramsey

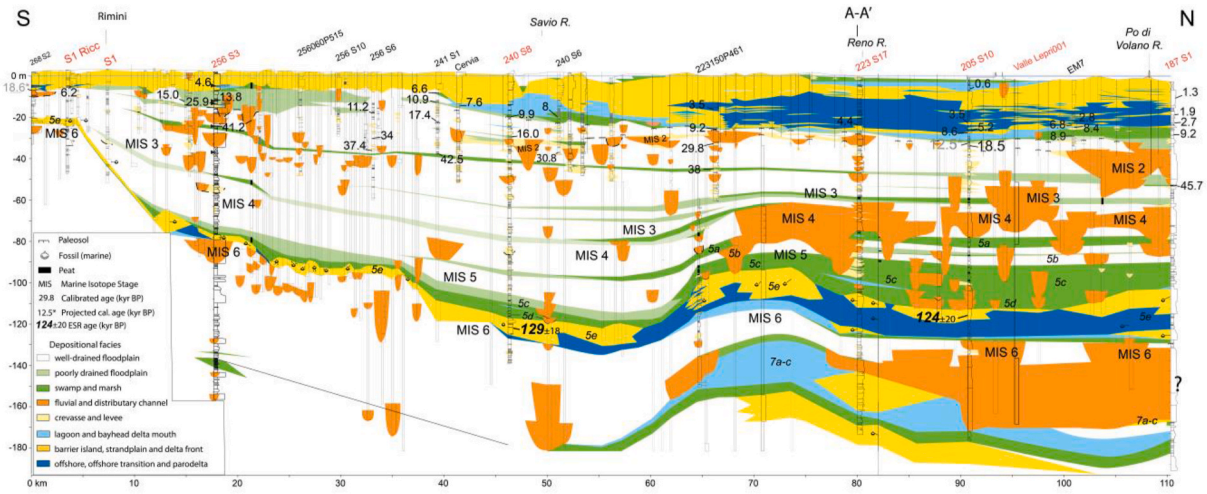

Fig. 5. – Mid-Late Pleistocene (MIS 7 to Present) stratigraphy of the Po Basin depicted in a cross-section running along the Adriatic coast (modified after Campo et al., 2020). See Fig. 1 for location.

Table 1
– Details on radiocarbon dates from cores 184S2, 184S5, 184S9, 184S13, 184S14 and 184S15.

Core	Lab	Material	depth (m)	^{14}C age	Calibrated age (mean ± 2σ)	Lab code
184S2	KIGAM	wood	5.1	868 ± 26	760 ± 40	KGM-OWd230534
184S2	KIGAM	wood	6.2	1286 ± 26	1225 ± 35	KGM-OWd230535
184S2	KIGAM	wood	11.1	4557 ± 31	5175 ± 95	KGM-OWd230536
184S2	KIGAM	wood	19.2	8974 ± 52	10130 ± 200	KGM-OWd220087
184S2	KIGAM	wood	20.95	8977 ± 51	10140 ± 200	KGM-OWd220088
184S2	KIGAM	wood	21.5	12034 ± 65	13920 ± 160	KGM-OWd220089
184S2	KIGAM	wood	23.8	10072 ± 53	11615 ± 265	KGM-OWd220090
184S2	KIGAM	wood	28.2	NaN	>54364	KGM-Owd220091
184S5	KIGAM	wood	4.2	2491 ± 28	2585 ± 75	KGM-OWd230541
184S5	KIGAM	wood	14.1	13370 ± 66	16090 ± 220	KGM-Owd220093
184S9	KIGAM	wood	16.55	6977 ± 36	7810 ± 60	KGM-OWd230542
184S9	KIGAM	wood	19.1	23249 ± 153	27500 ± 260	KGM-Owd220103
184S9	KIGAM	bulk sediment	23.95	45850 ± 782	48300 ± 2100	KGM-OWd220105
184S13	KIGAM	wood	8.6	2387 ± 29	2405 ± 70	KGM-OWd230546
184S13	KIGAM	bulk sediment	19.75	37579 ± 267	42100 ± 150	KGM-OSa230065
184S14	KIGAM	peat	22.05	47435 ± 907	50300 ± 3060	KGM-OWd220115
184S15	KIGAM	bulk sediment	7.5	7299 ± 52	8105 ± 120	KGM-OSa220045
184S15	KIGAM	wood	18.1	27285 ± 197	31320 ± 320	KGM-OWd220119

and Lee, 2013) with the IntCal 20 curve (Reimer et al., 2020).

Three sand samples were collected with a Shelby sampler from cores 184S2 and 184S15 (see Table 2) to be dated through the IRSL method. About 1 dm^3 of bulk sediment was collected in a darkroom from the innermost part of each sample, as equivalent dose (D_E), whereas sediments below and above D_E were sampled for environmental Dose Rate (D_{Ra} and D_{Rb}). An additional sample was taken and stored in a waterproof container to measure the moisture of the sediment. All samples, packed in light-proof containers, were shipped to the Utah State University Luminescence Laboratory, where they were prepared and analyzed. The 0.075–0.150 mm fraction was selected from D_E samples through wet sieving and treated with hydrogen peroxide, to remove organic matter, and with 10% hydrochloric acid to remove carbonates. Sodium polytungstate (2.58 g/cm^3) was used to isolate feldspar grains from heavy minerals and quartz. Luminescence dating followed the single-aliquot regenerative-dose (SAR) procedure for potassium feldspar dating in which post-infrared stimulated luminescence (pIR IRSL) measurement at 250 °C followed IR stimulation at 50 °C, both over 100s (Thomsen et al., 2008; Buylaert et al., 2009). Measurements were conducted on a Risø TL/OSL Model DA-20 reader using IR emitting diodes (875 nm) and signal detection through Schott BG-39 and Corning 7–59 filters (320–450 nm). The resultant DE data are fit with a saturating exponential curve. The pIR IRSL age is calculated by correcting for fading (loss of signal with time) using the method of Auclair et al. (2003) and the age correction model of Huntley and Lamothe (2001).

Dose-rate calculations were determined by chemical analysis of the U, Th, K and Rb content using ICP-MS and ICP-AES techniques and conversion factors from Guérin et al. (2011). Internal grain beta dose rate was determined assuming 12.5% K (Huntley and Baril, 1997) and 400 ppm Rb (Huntley and Hancock, 2001) attenuated to grain size using

Table 2
– Details on IRSL dates from cores 184S15 and 184S2.

Core	Depth (m)	Num. of aliquots	Dose Rate (Gy/Ka)	Equivalent Dose ± 2σ (Gy)	ISRL age, ±1σ (ka)	Fading Rate	USU code
184S15	87.45	9(10)	2.19 ± 0.10	795.81 ± 90.01	**363.9 ± 41.3**	1.75 ± 1.03 (n = 8)	USU-4289
184S15	110.25	10(11)	2.99 ± 0.15	1230.80 ± 168.64	**411.9 ± 49.5**	1.66 ± 0.90 (n = 3)	USU-4290
184S2	76	9(10)	2.94 ± 0.14	467.33 ± 84.54	**158.9 ± 21.3**	1.48 ± 0.6 (n = 7)	USU-4291

Mejdahl (1979). Alpha contribution to dose rate determined using an efficiency factor, 'a-value', of 0.15 ± 0.015 after Balescu and Lamothe (1994; see also Durcan et al., 2015). The contribution of cosmic radiation to the dose rate was calculated using sample depth, elevation, and latitude/longitude following Prescott and Hutton (1994). Dose rates are calculated based on water content, sediment chemistry, and cosmic contribution (Aitken and Xie, 1990; Aitken, 1998).

3.3. Pollen analysis

Pollen analysis was carried out on 107 samples throughout core 184S15. The amount of sediment treated varied according to lithology, 1 g peaty sediment to 5 g sandy/silty sediments. Pollen extraction followed the standard procedure (Magri and Di Rita, 2015), including HCl (37%), HF (40%), and hot NaOH (10%). After the chemical treatment, pollen samples were sieved in ultrasonic bath (CNCtech FTS 360) at 40 KHz for 10 min to remove particles <5 μm. Pollen concentration values were estimated by adding *Lycopodium* tablets to a known weight of dry sediment in each sample.

The identification of pollen was performed at magnifications of×400, ×630 and ×1000 under a Zeiss Axiolab A1 light microscope, with the aid of pollen atlases (Reille, 1992; Beug, 2004) and online databases (Non-Pollen Palynomorph Database, The Global Pollen Project, and Paldat-Palynological Database). A minimum of 150 pollen grains per sample were identified, except for pollen-poor samples (concentration <250 grains/g sediment), where a sum of at least 100 grains was reached. Pollen spectra with counts of upland pollen <100 grains were not represented. Pollen percentages were calculated on a base sum of terrestrial plants.

A synthetic pollen diagram compares the vegetation dynamics of arboreal taxa vs herbs with the stratigraphical and palaeoecological information. *Pinus* percentages are shown within the arboreal pollen synthetic diagram. In addition, four ecological groups are presented, including mixed oak forest, evergreen vegetation, montane trees, and riparian trees. The mixed oak forest comprises deciduous *Quercus*, *Carpinus betulus*, *Corylus*, *Ulmus*, and *Tilia*, along with less abundant broadleaved species. The evergreen vegetation is characterized by evergreen *Quercus* and *Olea*, with only sporadic occurrences of thermophilous elements like *Phillyrea*, *Ilex*, and *Buxus*. Montane trees consist of *Abies*, *Picea*, and *Fagus*. The riparian group is mainly composed of *Alnus*, *Salix*, and *Fraxinus*.

3.4. Meiofauna analysis

A total of 216 samples of ca. 100g were collected along core 184S15 for the analysis of meiofauna (benthic foraminifers and ostracods) to support and improve facies characterization. Samples were oven-dried for ca. 8 h at 60°, weighted and then soaked in a water and 4% hydrogen peroxide solution for ca. 8 h to allow complete disaggregation of the sediment. Afterwards, the sediment was washed through a 63 μm sieve, dried and weighted again according to the standardized methodology (Amorosi et al., 2014). Subsequently, the sediment was dry-sieved at 125 μm and a representative portion of the coarser fraction, separated using a micro-splitter, was quantitatively analyzed under an optical microscope. If possible, for each sample at least 300 specimens of benthic foraminifers and 100 valves of ostracods were identified and counted. In case the sample was depleted in fossils, the entire >125 μm fraction was examined. Taxonomic identification was based upon original species description (Ellis and Messina, 1940, 1952) and selected papers mainly focused on the Po-Adriatic area (e.g. AGIP, 1982; Jorissen, 1988; Barbieri and Vaiani, 2018). The (paleo)ecological and (paleo)environmental meaning of taxa was inferred from multiple papers based on modern assemblages (e.g. Athersuch et al., 1989; Henderson, 1990; Jorissen, 1988; Coccioni, 2000; Debenay et al., 2000; Meisch, 2000; Serandei Barbero et al., 2004; Murray, 2006).

To optimize the meiofauna dataset, species' frequencies are here reported following abundance categories previously adopted for the Po Delta area (Amorosi et al., 2019): abundant (>30%), common (30-10%) and scarce (<10%).

3.5. Subsidence-rates calculation

Subsidence rates, averaged over different periods, were calculated from individual cores along section AA' using lagoon and beach deposits, which accumulated close to the coeval sea-levels, as reference horizons (Bruno et al., 2020). The calculation of subsidence rates (SR) for a selected time interval (Δt) between the time of deposition (t_d) and the Present (t_0) was based on Eq. (1):

$$SR(\Delta t) = (Z_{td} - Z_{t0}) / \Delta t \quad (1)$$

where Z_{td} is the elevation of the stratigraphic marker at the time of deposition and Z_{t0} is the present elevation (see supplementary data). As sediment accumulation in back-barrier environments presumably took place in shallow water bodies (<2 m in Amorosi et al., 2004), an error of ±1 m was considered in SR calculation. An error of ±2 m was considered for beach deposits (Rovere et al., 2016). For the estimation of sea-level at the time of deposition of lagoon and beach horizons, we referred to Ferranti et al. (2006), Kopp et al. (2009), Dutton et al. (2009, 2015), Bowen (2010), Rovere et al. (2011), Raymo and Mitrovica (2012), Zazo et al. (2013), and Rohling et al. (2014). Considering the highest and the lowest sea-level estimations, we obtained a maximum and a minimum value of subsidence. Then we calculated the mean value and the standard deviation. The calculated subsidence rates include the contribution of the tectonic load and sediment compaction. The relative role of these two processes is not assessed in this paper.

4. Results

4.1. Depositional facies associations

Based on the reference cores 184S2 and 184S15 (Fig. 6), a brief description of continental to paralic facies associations is presented here. Coastal and marine facies, reported in several cores considered in this work, are described according to Amorosi et al. (1999, 2004, 2021).

4.1.1. Fluvial and distributary channel facies association

This facies association is composed of medium to coarse sand bodies with erosional lower boundary and fining-upward (FU) grain-size trend. Towards the basin margin, sands are replaced by gravels, with locally imbricated cobbles or pebbles. Thickness is > 3 m. Meiofauna is absent and wood fragments are seldom encountered.

Coarse-grained deposits, with erosive base and FU grainsize trend are interpreted as fluvial-channel (gravel, sand) or distributary channel (sand) sediment bodies (Allen, 1963; Miall, 1985, 1996; Bridge, 1993). These latter are distinguished by their lower width and slightly lower grain size and thus cannot be easily revealed by the analysis of a single core.

4.1.2. Crevasse and levee facies association

This facies association includes sand bodies (fine to medium sand), with either FU or coarsening-upward (CU) trend, and sand-mud alternations. Thickness is < 3 m. These deposits are barren of meiofauna, while wood fragments are locally observed.

Sand bodies with FU trend are interpreted as crevasse-channel deposit, whereas those with CU trend are referable to crevasse splays. Sand-mud alternations may reflect multiple episodes of overbank sedimentation close to an active channel and are interpreted as channel-levee deposits (Alexander and Prior, 1971).

4.1.3. Well-drained floodplain facies association

This facies association is dominated by varicolored silt and clay, with

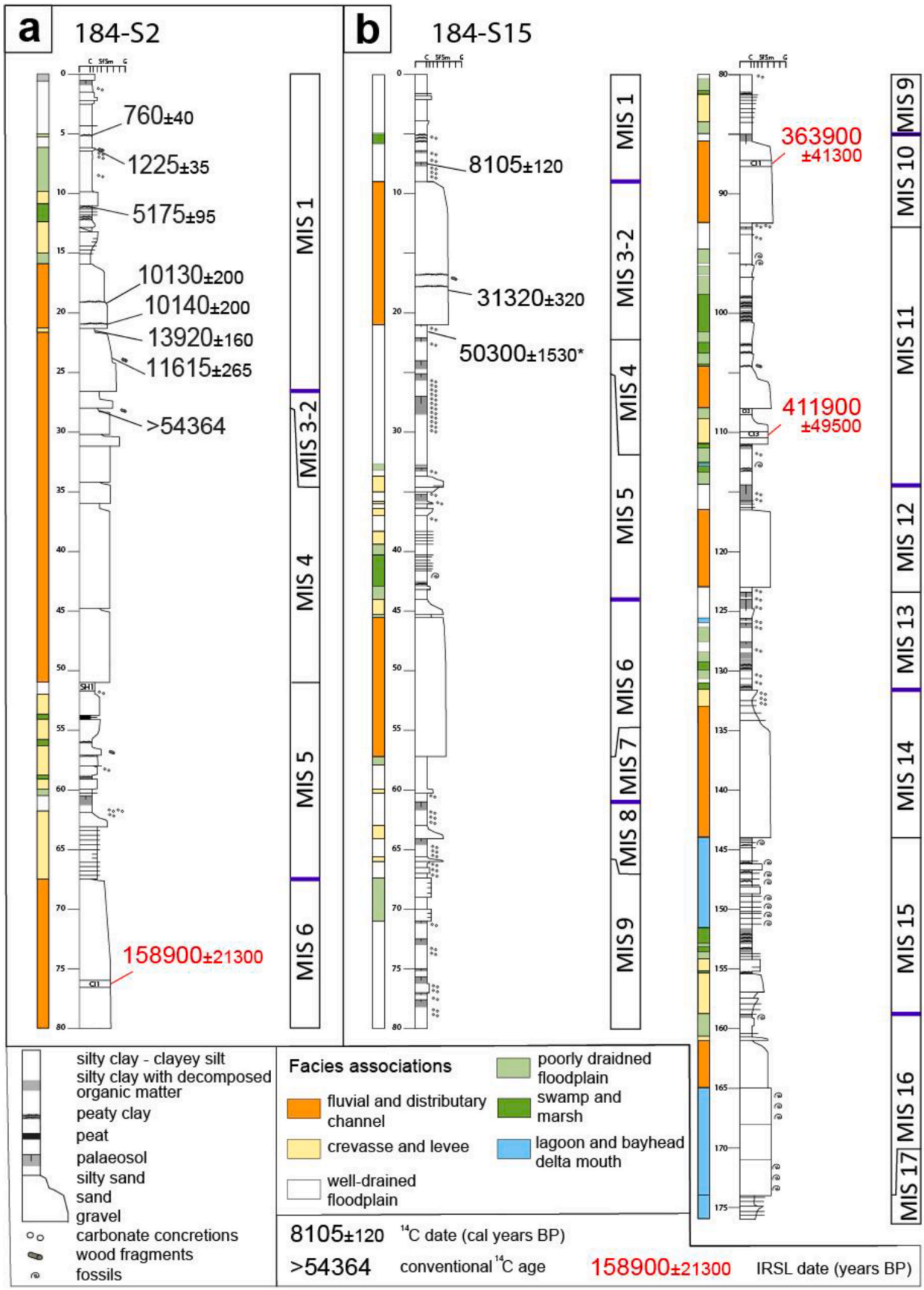

Fig. 6. – Facies interpretation and absolute ages of cores 184S2 and 184S15. Location in Fig. 1. The radiocarbon date with an asterisk is projected from a nearby core (see Table 1 for details).

carbonate concretions and iron oxides, marked by the rhythmical alternation of dark brown and whitish horizons. Carbonate concretions are abundant in whitish horizons. Thickness may exceed 10 m. These deposits are typically barren of meiofauna, with the exception of one sample containing abundant valves of *Pseudocandona* cf. *albicans* and rare *Mixtacandona* sp.

The dominance of mud suggests deposition in a low-energy floodplain environment (Collinson, 1978), occasionally hosting ponds, as testified by the presence of hypohaline and freshwater ostracod species (Meisch, 2000). Couplets composed of dark and whitish horizons are interpreted as paleosols resulting from exposure periods of a few thousand years (Inceptisols, Buol et al., 2011; Bruno et al., 2022).

4.1.4. Poorly drained floodplain facies association

This facies association is composed of soft grey silt and clay, with faint horizontal lamination and rare carbonate concretions. Thickness is < 3 m and locally a monospecific ostracod fauna composed of *Pseudocandona* cf. *albicans* occurs.

Soft grey muds are interpreted as deposited in a low-energy floodplain environment with water table fluctuating close to the topographic surface (Tentori et al., 2022). The rare occurrence of hypohaline ostracods preferring stagnant conditions (Henderson, 1990; Meisch, 2000) is consistent with this interpretation.

4.1.5. Swamp/marsh facies association

This facies association is composed of very soft and dark grey clays, rich in organic debris and marked by peat horizons. Thickness ranges between a few dm and ca. 5 m. Abundant valves of *Pseudocandona* cf. *albicans*, occasionally accompanied by common to scarce *Candona neglecta* and *Mixtacandona* sp., are locally observed. Few samples include a different meiofauna: ostracods show a co-dominance of *Pseudocandona* cf. *albicans* and *Cyprideis torosa* with scarce *Heterocypris salinus*, while the foraminiferal assemblage exhibits abundant *Ammonia tepida* (some of which deformed) with scarce *Ammonia parkinsoniana* and *Haynesina germanica*.

These deposits are interpreted as formed in submerged freshwater-hypohaline environments, such as swamps and marshes according to the abundance of *Pseudocandona* cf. *albicans* that thrives on organic-rich, stagnant bottoms (Henderson, 1990; Meisch, 2000). A slight increase in salinity may lead to the colonization of euryhaline species (*C. torosa* and the observed foraminiferal species; Athersuch et al., 1989; Murray, 2006). The sporadic absence of the meiofauna may reflect reducing conditions that favored the preservation of organic matter (Diessel, 1992; Richardson and Vepraskas, 2001; Stolt and Rabenhorst, 2011; Bruno et al., 2019). Laterally continuous successions (tens of km) of this facies association are interpreted to have formed as parts of wider bay-head- or upper-delta plain environments.

4.1.6. Lagoon and bay-head delta mouth facies association

This facies association is composed of soft grey muds characterized by a rich meiofauna, composed of ostracods and benthic foraminifers. Specifically, the ostracod fauna shows abundant *Cyprideis torosa*, scarce to common *Leptocythere bacescoi* and few valves of *Cytherois fischeri* and other *Leptocythere* species, such as *L. ramosa* and *L. macella*. As for benthic foraminifers, *Ammonia tepida* and *Ammonia parkinsoniana* are dominant, along with common to scarce specimens of *Haynesina germanica* and *Cribroelphidium* and *Porosononion* species. Few miliolids (mainly *Quinqueloculina seminulum*) and hyaline epiphytic taxa are seldom encountered. Thin fine-sand intercalations are locally observed and show lower species diversity (almost only *A. tepida* and *A. parkinsoniana* are found along with few valves of *C. torosa)*. This facies association includes sand bodies, 2–8 m thick, with a coarsening-upward trend (from fine to coarse sands). The base is either sharp or erosional, whereas the top is sharp. Vegetal remains, wood fragments and rare fragments of mollusc shells, are seldom encountered.

Soft grey muds containing euryhaline to brackish-marine ostracods and foraminifers (e.g. Athersuch et al., 1989; Murray, 2006) are interpreted as deposited in water bodies in partial communication with the open sea, such as lagoons, as a part of lower delta plains or outer estuaries. The observed taxa and low species diversity within fine-sand intercalations suggest a local increase in river input. Sand bodies with rare mollusc fragments are interpreted as bay-head delta mouths.

4.1.7. Barrier island, strandplain and delta front facies association

This facies association consists of laterally continuous sediment bodies elongated parallel to the modern Adriatic coastline, made up mainly of well-sorted, fine to medium sand. The thickness is highly variable, from a few meters to ~15 m, and plant debris are commonly observed. Ostracods and foraminifers (e.g., *Cushmanidea turbida*, *Semicytherura incongruens*, *Ammonia beccarii* and *Elphidium crispum*) showing evidence of abrasion and dissolution are locally encountered (Amorosi et al., 2004, 2017; Campo et al., 2017). Sand bodies may show an erosional lower boundary, often associated with a lag of reworked shells of brackish and shallow-marine mollusks, or a gradual base, with sharp top and CU trend.

These sand bodies are interpreted as deposited in a high-energy coastal environment, such as a barrier island, a strandplain or a delta front, with hydraulic sorting by waves and longshore currents (Amorosi et al., 1999, 2004, 2021). Sand bodies with erosive base and a poorly preserved shallow-marine meiofauna transported from nearby environments, are interpreted as transgressive barriers. The shell-rich lag at the base results from wave erosion and reworking during barrier retreat (Swift, 1968). Sand bodies with gradational base and coarsening upward trend are interpreted as deposited in a context of shoreline and delta progradation. The absence of macrofossils coupled with relatively high amounts of plant debris reflect proximity to fluvial mouths.

4.1.8. Prodelta, offshore-transition and offshore facies association

This facies association is composed of soft grey mud with thin intercalations of very fine to silty sand. A shallow-marine fossil assemblage, is typically retrieved. Particularly, relatively thin horizons (<3 m), with a diversified meiofauna, including several species of *Callistocythere, Semicytherura*, *Adelosina*, *Cribroelphidium, Elphidium*, *Quinqueloculina*, *Triloculina* and *Textularia*, and associated bioturbation, are in general overlain by thicker (up to 20 m) mud packages, with opportunistic species (e.g. *Varicorbula gibba*, *Palmoconcha turbida*, *Leptocythere ramosa*, *Ammonia parkinsoniana*, *Ammonia tepida*, *Nonionella turgida*) and thin organic-matter-rich horizons.

This mud-dominated facies association includes the most distal facies recognized in this study. Muds with thin-bedded sand intercalations are interpreted as offshore-shoreface transition or prodelta-delta front deposits, sand beds resulting from storm events or river floods, respectively. Bioturbated deposits with a diversified meiofauna, are typical of offshore conditions (Barbieri et al., 2021). Prodelta facies, instead, include opportunistic species able to tolerate stressed marine conditions with organic matter and sediment input related to major river floods (e.g. Scarponi and Kowalewski, 2007; Scarponi et al., 2014; Barbieri et al., 2021; Rossi et al., 2021).

4.2. Stratigraphy of cores 184S2 and 184S15

4.2.1. Core 184S2

Core 184S2, 80-m long, is composed of two fluvial-channel sand bodies that alternate with finer-grained intervals (Fig. 5A). The lower sand body is 12.5 m thick (from 80 to 67.5 m depth), and is composed of coarse to medium sand, with FU tendency. This sand body, IRSL-dated to MIS 6, is overlain by a 16 m-thick horizon dominated by channel-related facies associations, with swamp peaty mud intercalations. A paleosol was observed at 60.5 m depth. The thick interval between 51 and 16 m depth is composed of fluvial-channel sand. A wood sample collected at 20.2 m yielded an age beyond the ^{14}C window (>53364 years BP), whereas the uppermost 10 m of the sand body encompass the

Pleistocene-Holocene transition (10–13 ka BP). The Holocene succession is mainly composed of mud, with few sandy silt intercalations. Poorly drained floodplain and swamp facies associations are observed at depth >5.7 m, whereas the overlying layers are composed of well-drained floodplain mud.

4.2.2. Core 184S15

Core 185S15, 176-m long, is composed of sand-mud alternations at the decameter scale (Fig. 5B). Paleoecological analyses indicate an overall shallowing-upward trend, supported by the vertical stacking of: (i) a lower interval (174-144 m depth) with an abundant brackish meiofauna (lagoon facies association), with subordinate swamp/marsh, poorly drained floodplain and channel-related deposits; (ii) a thick unit (144-40 m depth) dominated by freshwater hypohaline ostracods (swamp facies association), alternating with increasingly thick floodplain deposits, and (iii) an upper interval (40-0 m depth) consisting predominantly of a well-drained floodplain deposits, with no fossils and abundant pedogenized horizons (paleosols), especially between 36 and 21 m.

Mud-prone intervals are separated by seven sand bodies with thickness ranging between 5 and 28 m. The deepest one, from 174 to 165 m, overlying silty sand containing a brackish meiofauna was inferred to represent a prograding bay-head-delta mouth succession. The overlying six sand bodies, at depth <165 m, are 3.5–12 m-thick, barren in fossils, and were interpreted as fluvial or distributary channel deposits.

4.3. Palynostratigraphy of core 184S15

The pollen record of core 184S15 reveals alternating pollen-rich and sterile intervals, generally reflecting the lithology of the sequence. Pollen concentration and preservation state vary along the core, depending on taphonomic conditions, sedimentation rates, and oxidizing processes. The sand bodies interpreted as fluvial or distributary channel facies associations were consistently sterile across the succession. The sandy-silt layers associated with the crevasse and levee facies, as well as the silty-clay layers of the poorly drained and well-drained floodplain facies associations usually exhibited low pollen concentrations (250–1000 grains/g sediment), locally with damaged and/or corroded pollen grains. Optimal pollen preservation and high pollen concentration values (10^3–10^4 grains/g sediment) were found in organic-rich clayey and peaty sediments corresponding to swamp and freshwater marsh facies.

Due to such heterogeneous sedimentary conditions, the pollen record appears discontinuous, being composed of 72 counted samples and 35 sterile samples. Eight distinct forest phases were detected and ascribed to interglacial periods, while vegetation corresponding to glacial periods is missing. All interglacial phases appear to be truncated in their terminal parts due to erosion likely related to the following glacial periods.

Crucial biostratigraphic information is provided by the occurrence of regionally extinct taxa, including *Zelkova*, *Pterocarya*, *Carya*, and *Tsuga*. By combining this information with the dynamics and composition of the vegetation, it was possible to assign the forested phases to known interglacial periods.

The vegetation phases of core 184S15 are related to specific Marine Isotope Stages (MIS), discussed in relation to the sedimentary facies and IRLS dates, and compared with other published pollen records from the Po Plain and other European sites (Fig. 7).

MIS 1: The forested phase at 2–6 m depth is dominated by deciduous *Quercus*, accompanied by a diverse mix of broadleaved taxa, mainly

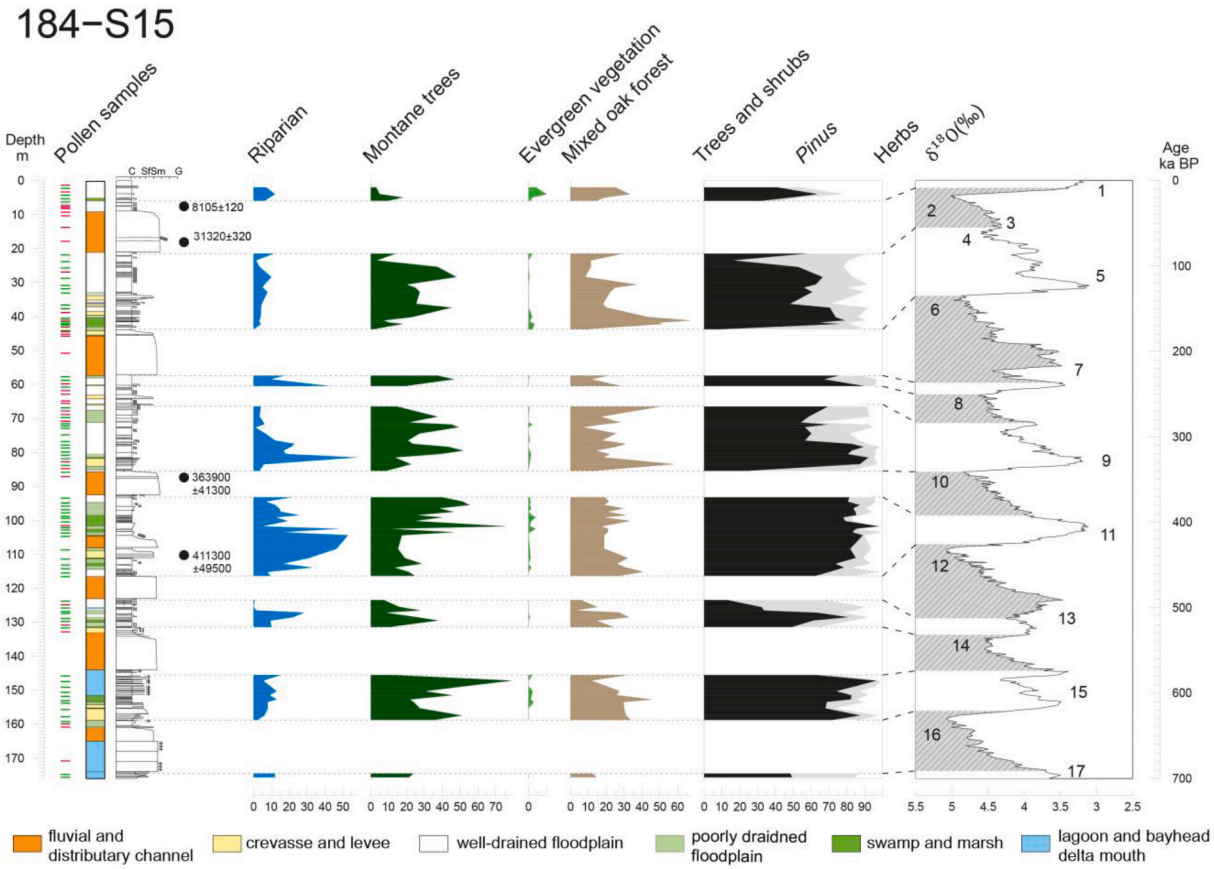

Fig. 7. – Synthetic pollen record from core 184S15 and correlation with the stacked $\delta^{18}O$ curve by Lisiecki and Raymo (2005). Numbers indicate Marine Isotope Stages. Dashes indicate the location of sterile (red) and counted (green) pollen samples. The pollen record includes a cumulative diagram with arboreal pollen, *Pinus*, and herbs, as well as four main ecological groups (see Methods).

Corylus, *Ulmus*, and *Ostrya*. Among herbs, Cichorieae and Amaranthaceae are the most represented taxa. The pronounced thermophilous evergreen component, mainly *Olea* and evergreen *Quercus*, and the concomitant decrease of *Abies*, suggest a Mid–Late Holocene age (Wick and Möhl, 2006; Di Pasquale et al., 2014; Magri et al., 2015). This chronological frame is confirmed by the radiocarbon date (8105 ± 120 cal years BP) at 7.5 m depth.

MIS 3–5: The forested phase between 21 and 44 m depth is found below the thick sand body assigned to MIS 2 and 3, as indicated by the radiocarbon date (31320 ± 320 cal years BP) at 18.1 m depth. The vegetation dynamics is characterized by three distinct peaks in arboreal pollen percentages, marked by prominent increases in mixed oak forest at ca. 21, 31, and 41 m, respectively.

The lowermost peak shows the highest percentage values of mixed oak forest throughout the record, along with appreciable values of evergreen trees, such as *Olea*. The development of this thermophilous vegetation corresponds to organic-rich clays associated with a swamp and freshwater depositional environment that progressively shifts to poorly drained floodplain deposits with alternating sandy crevasse-levee deposits. The vegetation composition suggests prominent warm and humid climatic conditions that can be ascribed to the MIS 5e sub-stage. This correlation is supported by the last occurrence of pollen of *Zelkova*, a regionally extinct taxon that gradually disappeared from the Italian Peninsula during the Late Pleistocene (Follieri et al., 1986; Magri et al., 2017). In northern Italy, it shows its last occurrence in several pollen records from the Po Plain during MIS 5e (Amorosi et al., 2004; Marcolla et al., 2021).

After this warm phase, a decrease in mixed oak forest is accompanied by a rise of montane taxa (*Abies* and *Picea*), indicative of cooler climatic conditions (Magri, 1999; Follieri et al., 1986; Pini et al., 2009, 2010). This cooling trend intensifies in the interval 37-35 m, resulting in the decline in both montane and thermophilous broadleaved taxa, along with an increase in *Pinus* percentages. This vegetation dynamics, corresponding to the occurrence of a paleosol, is consistent with the climate oscillation associated to sub-stage MIS 5d. Following this decline in tree cover, a progressive forest recovery culminates with a peak in mixed oak forest at 31 m, reflecting a shift towards well-drained floodplain depositional facies during milder climatic conditions, referable to sub-stage MIS 5c-5a.

Between 28 and 22 m, the pollen record shows a sharp decline in arboreal taxa and a significant increase in *Pinus* percentages, suggesting glacial climatic conditions that can be ascribed to MIS 4. In the stratigraphic record, this vegetation change correlates with the occurrence of stacked paleosols, reflecting prolonged periods with low sedimentation rates.

The forest expansion around 21 m depth shows the recovery of mixed oak forest, suggesting a shift towards warmer climatic conditions. This phase, with lower arboreal pollen percentages compared to the forested phases of MIS 5, is consistent with the relatively mild climatic conditions that characterized MIS 3. The record stops abruptly with an erosive surface, marking the base of a sand body assigned to the Last Glacial Maximum.

MIS 7: A third forested phase is identified between 56 and 61 m. This short-lived interval, corresponding to a well-drained floodplain facies, is characterized by high percentages of montane taxa, primarily *Abies*, with moderate values of mixed oak forest, suggesting temperate climatic conditions. Rising values of riparian trees, mainly *Alnus*, indicate increasing water availability. Considering the vegetation composition, indicating a cooler climate with respect to the forested phases of MIS 5e, this phase can be tentatively ascribed to an early sub-stage of MIS 7 (Fig. 7). It terminates abruptly with a thick fluvial sand body presumably deposited during MIS 6, a glacial period with extreme conditions that caused a large part of the interglacial deposits corresponding to MIS 7 to be eroded.

MIS 9: The fourth vegetation phase, ranging from 66 to 86 m, is characterized by two main forest expansions, presenting a few pollen grains of *Pterocarya*. The bottom forest phase, spanning 86 to 81 m, is characterized by a rapid growth of mixed oak forest, followed by a sharp increase in riparian trees. This vegetation dynamics aligns with a stratigraphic transition from fluvial channel facies, dated 363900 ± 41300 years BP, to a floodplain deposit with varying degrees of drainage, eventually culminating in swamp and freshwater marsh conditions around 81.5 m. At this depth, the prevalence of *Alnus* suggests the establishment of a wetland dominated by alder carr, followed by an increase in montane taxa (*Abies* and *Picea*) indicating a climate cooling trend. Palynological data related to this forested phase converge with sedimentological evidence and IRSL dating in depicting a landward shift of sedimentary facies, which occurred in response to a transgressive phase that can be assigned to the MIS 9e sub-stage. A second major forest expansion is detected in poorly drained depositional facies ranging from ca. 71 to 66 m depth. This phase is characterized by a complex mixed oak forest community that could be ascribed to the MIS 9a sub-stage. The vegetation reconstruction stopped at 66 m depth in correspondence of well-drained floodplain deposits with sterile paleosols and sands, probably deposited during the glacial period corresponding to MIS 8.

MIS 11: The fifth wooded phase, ranging from ca. 92–117 m, shows high and uniform arboreal pollen percentages, with relatively low values of *Pinus*. The mixed oak forest shows a stable profile throughout this interval, with slightly higher values at lower depths. Within this phase, the main vegetation change is marked by a sudden and considerable increase of riparian vegetation (mainly *Alnus*) detected across multiple peaty layers and culminating at ca. 104 m depth. Moving upwards, the riparian vegetation gives way to an increase in montane taxa (*Abies* and *Fagus*), alongside thermophilous deciduous and evergreen vegetation, suggesting the establishment of a new ecological setting with a lowland wooded environment at the transition from swamp depositional facies to floodplain deposits. This vegetation dynamics can be assigned to a single transgressive episode that led to the establishment of wetland environments, followed by a warm highstand phase characterized by dense alluvial forests. This single-pulse vegetation response can be ascribed to the period spanning from MIS 11e to MIS 11c substages. This chronological frame is also confirmed by the IRSL date of 411300 ± 49500 years BP obtained from the sand body sandwiched between wetland deposits and associated to crevasse-and-levee facies. The pollen record terminates abruptly with a shift to sterile sands suggesting that MIS 11b and MIS 11a sub-stage deposits were eroded away during MIS 10.

MIS 13: The forested phase detected approximately from 123 to 132 m is marked by a single and sharp increase in arboreal pollen percentages, observed within alternating swamp/freshwater marsh facies and poorly drained floodplain deposits This surge in tree cover consists of a peak in mixed oak forest and a concomitant increase in riparian taxa, suggesting warm and humid climatic conditions. Spotted occurrences of *Carya* align with the scattered presence of this taxon across the Italian Peninsula during MIS 13 (Russo Ermolli, 1994; Orain et al., 2013; Di Rita and Sottili, 2019). Based on this biostratigraphic evidence and vegetation composition, it is reasonable to assign this forested phase to an early phase of MIS 13, probably the MIS 13c sub-stage. The following forest decline, between 126 and 123 m, is characterized by the dramatic increase in *Pinus* percentages, corresponding to a sedimentological shift towards well-drained floodplain conditions characterized by repeated soil development. Both sedimentological and palynological evidence point to a change in environmental and climatic conditions that is consistent with the onset of a stadial period. Afterwards, the abrupt shift to sterile sands (probably referable to MIS 12), interrupts the pollen records and prevent the reconstruction of the vegetational landscape during the later stages of MIS13.

MIS 15: Between 144 and 159 m depth, the pollen record reveals a phase of prominent woodland cover marked by three distinct forest expansions. The bottom peak, reflecting mixed oak forest and montane taxa (mainly *Abies*), corresponds to sandy and silty sediments associated

to crevasse and levee deposits. The second forest expansion consists of mixed oak forest coupled with appreciable values of evergreen thermophilous elements, indicating warm climatic conditions. In the stratigraphic record, soft and dark grey clays with peaty horizons have been associated to submerged freshwater environments. During the third forest expansion, montane trees dominate, with *Abies* reaching its highest values throughout the sequence. This extensively forested phase corresponds to soft grey muds associated to lagoon, saltmarsh, and bayhead delta depositional facies. A recovery of mixed oak forests is found at around 145 m depth, preceding an abrupt interruption of the pollen record at around 145 m. Overall, this vegetation dynamics, describing subsequent expansions of tree populations with alternating montane/temperate trees and thermophilous deciduous taxa, reflects oscillating climatic conditions mirroring the $\delta^{18}O$ profile of MIS 15, with forest increases possibly corresponding to substages MIS 15e, 15c, and 15a, respectively.

MIS 17: The bottom vegetation phase is represented by few samples from silty sediments. This phase is characterized by moderate values of montane taxa (20–25%), primarily *Abies*, and modest percentages of mixed oak forests (10–15%). Evergreen elements are virtually absent. A thick bayhead-delta-mouth sand body abruptly interrupts the pollen profile. The vegetation composition reflects a partially forested environment under cool/temperate climatic conditions that is tentatively attributed to an interglacial phase of MIS 17.

4.4. Mid-Late Pleistocene and Holocene stratigraphy of the Po basin

The Mid-Late Pleistocene and Holocene stratigraphy of the Po Basin is depicted along two cross-sections: section AA' (Fig. 8), traced from land to sea for a total length of 109 km, and section B-B' (Fig. 9), N-S directed from the Apennine margin to the Po River, for 67 km (see Fig. 1 for location).

An overall shallowing-upward trend, from predominantly coastal deposits to exclusively alluvial facies, via paralic deposits of variable thickness, is observed in section AA'. Along individual cores, nearshore and paralic deposits thin upwards, whereas alluvial facies show an opposite trend (Figs. 6, 8 and 9).

In section AA', prominent wedge-shaped sediment bodies made up of coastal sands and shallow-marine muds occur at distinct stratigraphic levels, typically separated by alluvial sediments (Fig. 8). In the lower part of each wedge, coastal sands form relatively thin, poorly interconnected sediment bodies with a markedly retrogradational pattern. Upsection, sand bodies are more interconnected and stacked in an overall progradational trend. At the turnaround from retrogradation to progradation, sand bodies are thickest and typically amalgamated. Coastal sediments grade landwards into paralic (lagoon and swamp/marsh) and then alluvial sediments (Fig. 8).

The uppermost coastal wedge in Fig. 8 was radiocarbon dated to the Holocene (MIS 1), whereas the coastal wedge encountered about 100 m below was ESR dated to the Last Interglacial (MIS 5e). Based on pollen data from cores 184S15 (Figs. 7), 204S4 (Calabrese et al., 2008); 222S2 (Fusco et al., 2003) and 223S17 (Amorosi et al., 1999) and using the IRSL age of core 184S15 as a chronologic constraint for the MIS 9 coastal wedge, we assign the intervening wedges to MIS 7a-c and MIS 7e, respectively. Based on pollen data and IRSL ages from core 184S15 (Fig. 7), coastal sands beneath the MIS 9 coastal wedge are assigned to MIS 11 and MIS 13, respectively. Two coastal wedges, at depth >150 m close to the culmination of the Mirandola anticline (core GL5123, Fig. 8), are assigned to MIS 15 and MIS 17 based on pollen data from core 184S15 (Fig. 7). The chronologic attribution of the coastal deposit recognized in Core MIR (Fig. 8) is difficult due to the intense tectonic deformation of that region, which hinders reliable stratigraphic correlations based uniquely on geometric criteria.

With the sole exception of the MIS 7a-c coastal wedge, progressively older coastal deposits are encountered at increasing distances from the modern coastline. Particularly, the MIS 1 wedge extends ca. 20 km landward of the modern coastline, whereas the innermost MIS 5 and MIS 7e coastal sands are recorded ca. 35 km from the present-day coastline (core 204S17). The innermost MIS 9 and MIS 11 coastal deposits were observed 60 km away from the modern coastline (core 203S9), whereas the most landward position of MIS 13 coastal sands is ca. 85 km west of the present-day coastline. The innermost sands of the two coastal wedges assigned to MIS 15 and MIS 17 were encountered in core GL5123, ca. 95 km from the modern coastline. Paralic sediments show a consistent trend. Lagoon deposits are particularly abundant between the MIS 11 and MIS 9 coastal sands (see cores 203S9 and 203S11).

Based on this cyclic organization of facies, the Mid-Late Pleistocene succession was subdivided into a set of transgressive-regressive (T-R) cycles. The bounding surfaces (transgressive surfaces or TS) were traced at the base of coastal wedges, where aggradationally stacked alluvial deposits are overlain by retrogradationally stacked paralic and coastal deposits. To the west, the base of laterally extensive swamp/marsh or poorly drained-floodplain intervals represents the landward equivalent of the TS. Along single cores, the TSs invariably mark the base of sediment packages with deepening-upwards facies trends. Individual cycles are up to 55 m thick and thin out westward, toward the culmination of the Mirandola anticline.

In section BB' (Fig. 9), perpendicular to the main tectonic structures,

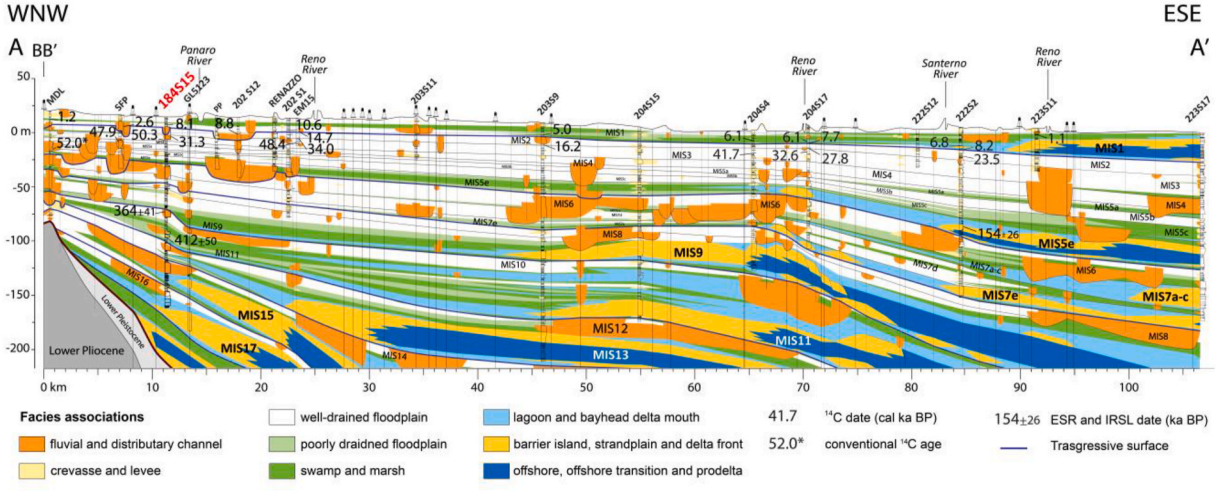

Fig. 8. Mid-Late Pleistocene and Holocene stratigraphy of the Po Basin depicted in a cross-section running along the Mirandola thrust system. Location in Fig. 1. For details on new ^{14}C and IRSL ages, see Tables 1 and 2

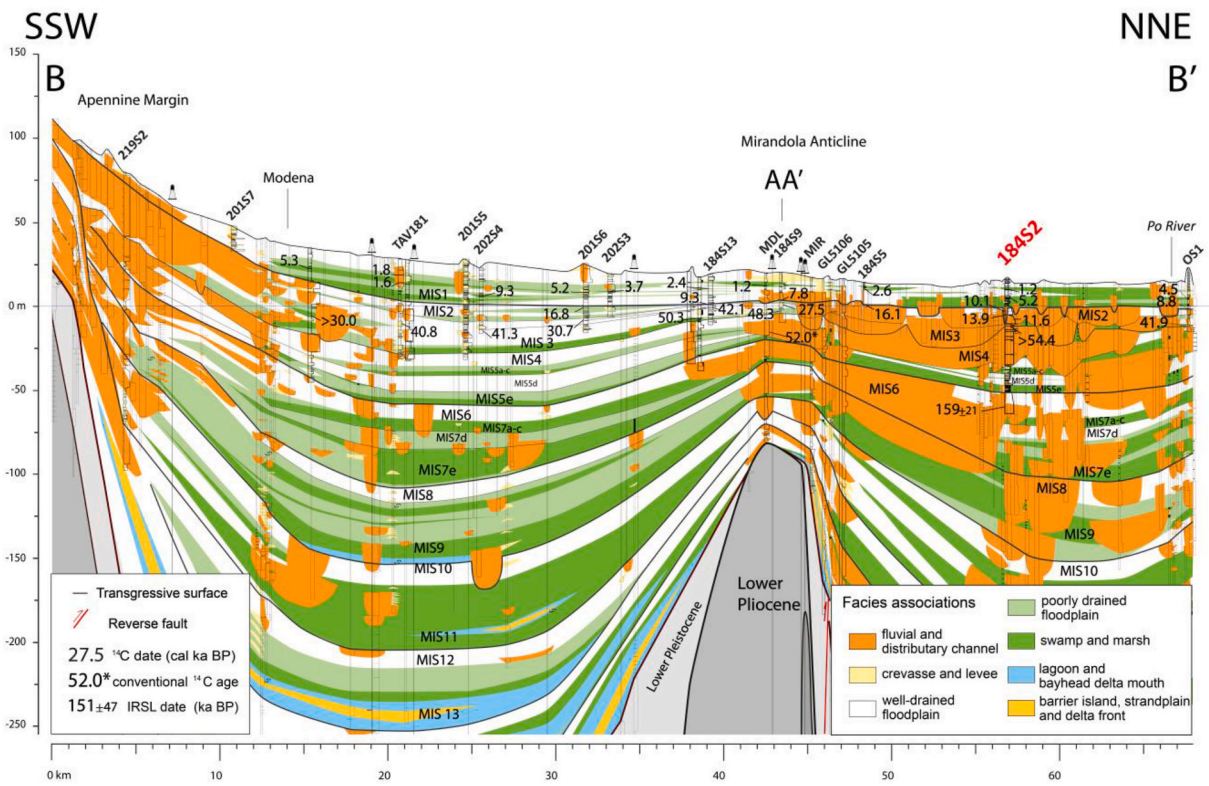

Fig. 9. Mid-Late Pleistocene and Holocene stratigraphy of the Po Basin along a N-S oriented cross-section transversal to the Apennine margin and to the Mirandola thrust system. Location in Fig. 1. For details on new ^{14}C and IRSL ages, see Tables 1 and 2

the sedimentary succession is folded close the Apennine margin and above the Mirandola thrust-related anticline, with a degree of deformation that increases with depth. The thickness of Middle Pleistocene to Holocene deposits is about 100 m close to the Apennine margin and above the Mirandola anticline, whereas it may exceed 300 m in syncline areas. The stratigraphic succession, 100 km landward of the modern shoreline, consists almost exclusively of alluvial and paralic deposits, with highly subordinate coastal deposits in the older stratigraphic intervals (Fig. 9). The landward equivalents of the T-R cycles illustrated in section AA' (Fig. 8) are composed, in their lower portions, by lagoon and swamp/marsh facies associations that are replaced upwards by alluvial facies associations. These latter are represented by thick fluvial channel-belts that are clustered close to the Apennine margin and in the axial portion of the plain, between the Mirandola thrust system and the modern Po River. Lateral to the fluvial channel-belt sand bodies, alluvial facies consist predominantly of floodplain muds. Lagoon and swamp/marsh intervals thin upwards, whereas the thickness and lateral extent of fluvial sand bodies increase upwards, with two 15-20 km-wide and 30-40 m-thick channel belts dated to MIS 6 (see IRSL age in core 184S2) and to the last glacial episode (MIS 4-MIS 2), respectively.

5. Discussion

The Po Basin fill is characterized by an overall shallowing-upward trend, from Pliocene and Early Pleistocene turbidites to Mid-Late Pleistocene and Holocene shelf, coastal and alluvial deposits. This tendency, documented in several regional stratigraphic studies during the last decades (Ricci Lucchi et al., 1982; Ori, 1993; Massari et al., 2004; Ghielmi et al., 2013), reflects the progressive filling of the basin and the transition from the underfilled to the overfilled stage (*sensu* Catuneanu, 2017). Within this general trend, local studies carried out in the central Po Plain (Amorosi et al., 2008) and beneath the modern coastal plain (Amorosi et al., 2004; Campo et al., 2020) documented the repeated alternation of fluvial/overbank and coastal/alluvial deposits in response to Milankovitch-scale 100 ka-cyclicity.

The stratigraphy of the late Quaternary succession of the Po Plain, reconstructed in this work on a basin scale along sections AA' (109 km long) and BB' (67 km long), highlights a similar trend of facies architecture, providing for the first time a detailed framework of Mid-Late Pleistocene stratigraphy and of its relationship with the underlying tectonic structures.

The overall shoaling-upward trend is punctuated at distal locations by a clearly detectable depositional cyclicity of coastal, paralic and alluvial systems (Fig. 8). More inland, depositional cycles include sharp swamp/marsh to alluvial or overbank to fluvial transitions (Fig. 9). Along-dip facies shifts for tens of km reflect the increased amplitude of glacio-eustatic oscillations after the Early/Middle Pleistocene Transition (Head and Gibbard, 2005, 2015), and were enhanced by the low gradients of the Po Plain and of the Adriatic shelf. The rhythmical occurrence of the T-R coastal wedges testifies to interglacial marine ingressions, followed by highstand deltaic and coastal progradation. The abundance of lagoon deposits during MIS 11 could reflect the exceptional length of the MIS 11 highstand (Loutre and Berger, 2003; Siddall et al., 2007; Zazo et al., 2013).

The superposition of the glacio-eustatic signal to the structurally controlled basin fill resulted in the progradational/aggradational stacking of T-R wedges, which migrated seawards through time (Figs. 8 and 10). The location of the MIS 7a-c coastal wedge, which does not comply to this trend, is possibly attributable to the relatively lower sea-level position during this interstadial compared to MIS 5e, MIS 7e and MIS 9 (Lea et al., 2002; Waelbroeck et al., 2002; Dutton et al., 2009; Rovere et al., 2011). On the other hand, MIS 13, MIS 15, and MIS 17 coastal sands at the time of maximum marine ingression accumulated 22, 33 and 35 km landward of the MIS 11 shoreline (Fig. 8), although maximum sea levels between MIS 13 and MIS 17 were lower than in MIS 11 (Rohling et al., 2014, Fig. 10). The overall seaward shift of facies, thus, is not related to sea-level change, but likely resulted from the high volumes of sediment supplied to the Po Basin from the two active

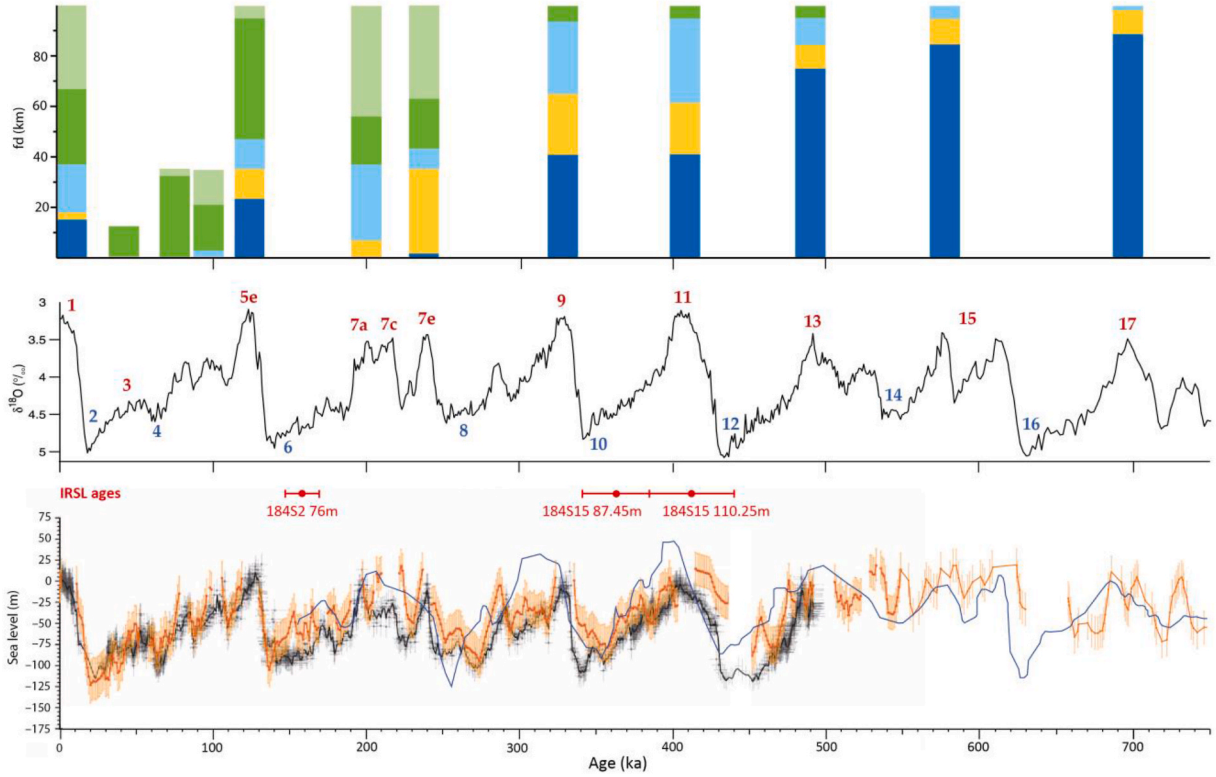

Fig. 10. – (A) Maximum inland location of depositional facies associations during the Mid-Late Pleistocene and Holocene interglacials and interstadials, reported as distance from the modern coastline and measured along section AA' (fd). Glacial and stadials are dominated by alluvial facies associations. See Figs. 6–9 for keys to facies associations. See text for details. (B) Global benthic stack in the last 750 ka (modified after Lisiecki and Raymo, 2005). (C) Sea-level oscillations in the Mediterranean (red), Red Sea (black) and Northern Atlantic (blue). Modified after Rohling et al. (2014).

orogens (Alps and Apennines), which overcame the rate of creation of accommodation space due to subsidence.

Subsidence rates calculated along section AA' vary from 0.2 mm/y, at the culmination of the Mirandola anticline, to ca. 1 mm/y beneath the Adriatic coast (Fig. 11 and Table 3). This seaward increase in subsidence rates might be related to different growth rates along the Mirandola anticline, or to the relative abundance of highly compressible paralic and marine sediments at distal locations. Higher growth rates in the landward sector of the Mirandola anticline could have enhanced the progressive seaward migration of facies. However, the available data are insufficient to discriminate the relative role of sediment supply and differential subsidence. Sediment budget calculations based and specific structural studies of the Mirandola thrust system are required to this aim.

Whereas the 100 ka-scale depositional cyclicity is a common tract in all alluvial-coastal systems worldwide (Liu et al., 2003; Busschers et al., 2005; Yao et al., 2020; Thanh et al., 2021), the long-term sedimentary evolution differs from a site to another on the basis of the local tectonic-geographic setting (DeCelles, 2012; Zhang et al., 2019). Alluvial and coastal plains developed in foreland basins fed by active thrust-belt orogens lie onto shallowing-upward sedimentary successions that show the transition from deep-marine to continental and coastal deposits, possibly with a final stage of terrace formation (Carter and Naish, 1998; Tropeano et al., 2002; DeCelles, 2012). In these settings, and in ancient successions (Bentham et al., 1992; Hampson, 2016), the shoaling upward trend has been illustrated at the Ma time scale. In this work, we recognized a similar trend, but at a finer resolution (100 ka) and imaged the progradational/aggradational stacking of T-R wedges, highlighting the interaction between the internal dynamics of the basin filling and the 100 ka-scale climate forcing.

6. Conclusive remarks

The sedimentary response of alluvial and coastal areas to Quaternary glacio-eustatic oscillations has been widely documented in the scientific literature. Most of the papers focused on the Late Pleistocene-Holocene transition, whereas only few works explored the evolution of alluvial and coastal systems during the Middle Pleistocene. Through the correlation of 43 cores and 168 well data, with the aid of pollen data and ^{14}C, ESR and IRSL ages, we reconstructed the Mid-Late Pleistocene and Holocene stratigraphy of the Po Basin, and the evolution of the Po-Adriatic alluvial-coastal system since MIS 17The results of this research can be summarized as follows.

- The Mid-Late Pleistocene and Holocene sedimentary succession of the Po Basin is composed of alluvial, paralic, coastal and shallow marine facies associations stacked in an overall shallowing-upward trend.
- This general trend is punctuated by a cyclic organization of facies given by the rhythmical occurrence of transgressive-regressive (T-R) coastal wedges, separated by alluvial deposits. Landwards, where coastal facies are highly subordinate, the depositional cyclicity is marked by the alternation of paralic (mainly swamp and freshwater marsh) deposits with alluvial (fluvial-channel and floodplain) facies associations.
- Superposition of the shoaling-upward trend with the higher-frequency depositional cyclicity resulted in an overall progradational/aggradational stacking of (T-R) coastal wedges.
- The overall shallowing-upward trend reflects the progressive filling of the basin due to high sediment supply which overcame the rate of creation of accommodation induced by subsidence. Differential subsidence, with increasing values towards the sea, may have enhanced the seaward migration of coastal facies.

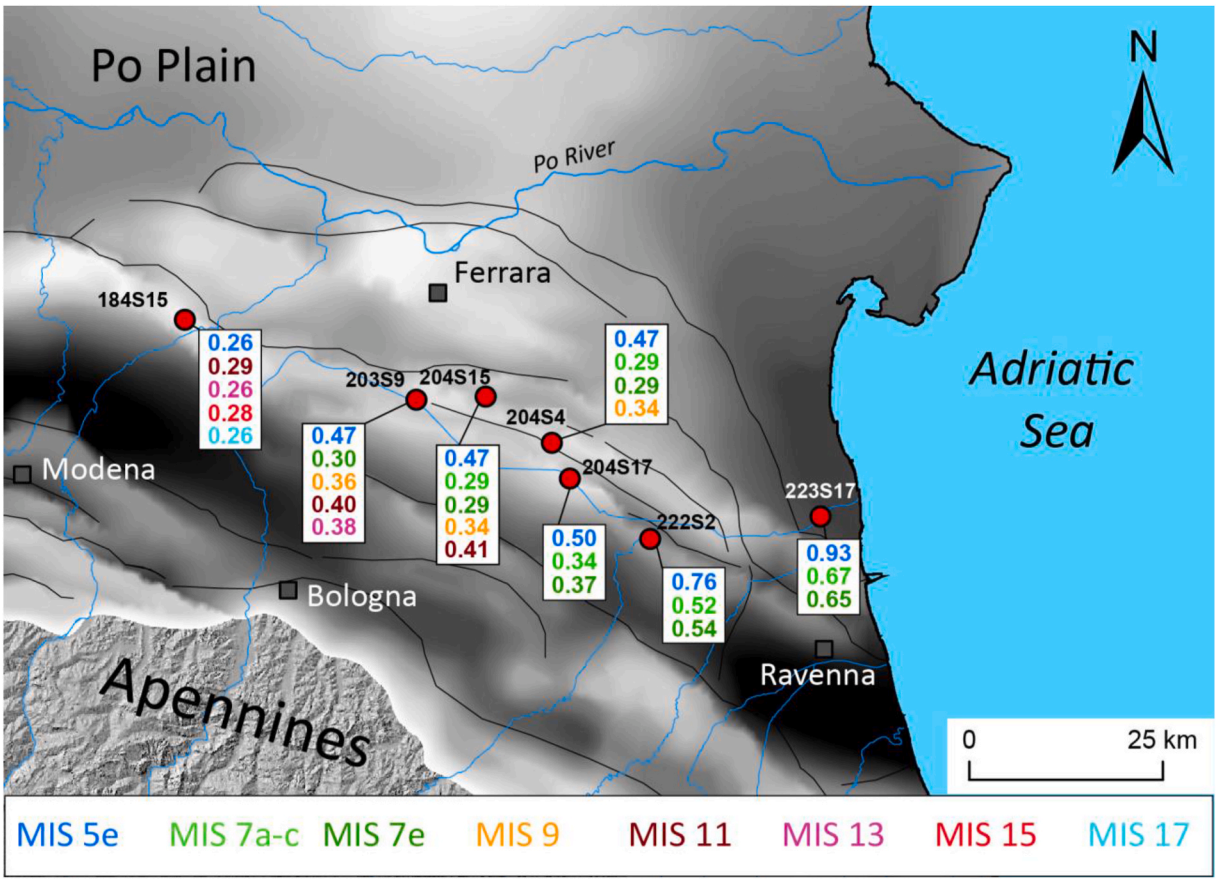

Fig. 11. – Subsidence rates measured in cores along section AA' and averaged over the last 122 ka (blue), 196 ka (light green), 240 ka (green), 323 ka (orange), 404 ka (burgundy), 494 ka (fuchsia), 621 ka (red) and 712 ka (light blue). Details on subsidence rates in Table 3.

Table 3
Subsidence rates, and associated errors, calculated for the time between the Interglacials and Interstadials indicated in the left column (MIS) and the Present. For the calculation, the displacement of stratigraphic horizons that accumulated at paleo sea levels has been considered (see section 3.5. for details). Sea levels for each MIS are from Kopp et al. (2009) (a), Hearty et al. (2007) (b), Dutton et al. (2015) (c), Waelbroeck et al. (2002) (d), Dutton et al. (2009) (e), Rohling et al. (2014) (f), Raymo and Mitrovica (2012) (g) and Bowen (2010) (h). For location of cores 184S15, 203S9, 204S15, 204S4, 204S17, 222S2 and 223S17, see Fig. 11.

MIS	Sea level at time of deposition (m)		Subsidence Rates (mm/y)						
	max	Min	184 S15	203 S9	204 S15	204 S4	204 S17	222 S2	223S17
5e	+9.4[a]	+6[b,c]	**0.26** ± 0.05	**0.47** ± 0.06	**0.47** ± 0.06	**0.47** ± 0.06	**0.50** ± 0.07	**0.76** ± 0.08	**0.93** ± 0.09
7ac	+10[d]	−18[e]			**0.29**±<0.01	**0.29**±<0.01	**0.34** ± 0.02	**0.52** ± 0.03	**0.67** ± 0.04
7e	+1[d]	−18[e]		**0.30** ± 0.06	**0.29** ± 0.02	**0.29** ± 0.02	**0.37** ± 0.03	**0.54** ± 0.04	**0.65** ± 0.04
9	+25[f]	−12.5[f]		**0.36** ± 0.07	**0.34** ± 0.07	**0.34** ± 0.07			
11	+13[g]	−1.5[h]	**0.29** ± 0.02	**0.40** ± 0.03	**0.41** ± 0.03				
13	+20[f]	−17[f]	**0.26** ± 0.04	**0.38** ± 0.05					
15	+40[f]	0[f]	**0.28** ± 0.01						
17	+30[f]	−10[f]	**0.26** ± 0.01						

- The cyclic arrangement of facies reflects high-amplitude glacio-eustatic oscillations since the Early/Middle Pleistocene Transition. Along-dip facies shifts driven by sea-level changes were enhanced by the low gradients of the Po Plain and of the Adriatic shelf.

The results of this study provide clues on the sedimentary response of a low-gradient costal systems to sea-level oscillation in a period, the Mid-Late Pleistocene, characterized by dramatic climate changes. Therefore, the data presented here may help in predicting the response of depositional systems to near future climate and eustatic changes.

Author contribut\ions

All authors made substantial contributions to this paper. Particularly, Luigi Bruno and Alessandro Amorosi, planned borehole drilling and core sampling for paleo-environmental (pollens and microfossils) and chronological (^{14}C, ESR and pollens) analysis. Luigi Bruno coordinated the drafting of the manuscript and wrote himself large part of the text. The PhD student Luca Demurtas, under the supervision of Luigi Bruno, created the stratigraphic cross sections, produced IRSL data in the lab directed by Tammy Rittenour and contributed to the drafting of the manuscript. Donatella Magri and Fabrizio Michelangeli produced and interpreted pollen data and wrote the relative section of the paper. Veronica Rossi, Stefano Claudio Vaiani and Amanda Vecchi produced and interpreted paleontological data and wrote the relative section of the paper. Tammy Rittenour coordinated lab activities for the production and interpretation of IRSL data. Wan Hong provided ^{14}C dates. Luigi Bruno revised the paper with

contributions from Alessandro Amorosi, Luca Demurtas, Donatella Magri, Fabrizio Michelangeli, Veronica Rossi, Amanda Vecchi and Stefano Claudio Vaiani. All authors approved the final version of the manuscript.

Declaration of competing interest

The co-author Donatella Magri is a member of the Editorial Board of *Quaternary Science Review* and was not involved in the editorial review or the decision to publish this article. The other authors declare that they have no known competing financial interests or personal relationships that could have appeared to influence the work reported in this paper.

Acknowledgments

This paper benefited from funds from the Italian Institute for Environmental Protection and Research, for the realization of the Geological Map of Italy to scale 1:50.000 (CARG project), sheet 184 “Mirandola”.

Data availability

Data will be made available on request.

References

AGIP, 1982. Foraminiferi Padani (Terziario e Quaternario), Milan.
Aitken, M.J., 1998. An Introduction to Optical Dating: the Dating of Quaternary Sediments by the Use of Photon-Stimulated Luminescence. Oxford University Press, New York, p. 267.
Aitken, M.J., Xie, J., 1990. Moisture correction for annual gamma dose. Ancient TL 8 (2), 6–9.
Alexander, C.S., Prior, J.C., 1971. Holocene sedimentation rates in overbank deposits in the Black Bottom of the lower Ohio River, southern Illinois. Am. J. Sci. 270 (5), 361–372.
Allen, J.R.L., 1963. The classification of cross-stratified units with notes on their origin. Sedimentology 2, 93–114.
Allen, G.P., Posamentier, H.W., 1993. Sequence stratigraphy and facies model of an incised valley fill; the Gironde Estuary, France. J. Sediment. Res. 63 (3), 378–391.
Amadori, C., Garcia-Castellanos, D., Toscani, G., Sternai, P., Fantoni, R., Ghielmi, M., Di Giulio, A., 2018. Restored topography of the Po Plain-Northern Adriatic region during the Messinian base-level drop—implications for the physiography and compartmentalization of the palaeo-Mediterranean basin. Basin Res. 30 (6), 1247–1263.
Amadori, C., Toscani, G., Di Giulio, A., Maesano, F.E., D’Ambrogi, C., Ghielmi, M., Fantoni, R., 2019. From cylindrical to non-cylindrical foreland basin: Pliocene-Pleistocene evolution of the Po Plain-Northern Adriatic basin (Italy). Basin Res. 31 (5), 991–1015.
Amadori, C., Ghielmi, M., Mancin, N., Toscani, G., 2020. The evolution of a coastal wedge in response to Plio-Pleistocene climate change: the Northern Adriatic case. Mar. Petrol. Geol. 122, 104675.
Amorosi, A., Colalongo, M.L., Fusco, F., Pasini, G., Fiorini, F., 1999. Glacio-eustatic control of continental–shallow marine cyclicity from late Quaternary deposits of the southeastern Po Plain, northern Italy. Quaternary research 52 (1), 1–13.
Amorosi, A., Forlani, L., Fusco, F., Severi, P., 2001. Cyclic patterns of facies and pollen associations from Late Quaternary deposits in the subsurface of Bologna. Geoacta 1, 83–94.
Amorosi, A., Colalongo, M.L., Fiorini, F., Fusco, F., Pasini, G., Vaiani, S.C., Sarti, G., 2004. Palaeogeographic and palaeoclimatic evolution of the Po Plain from 150-ky core records. Global Planet. Change 40 (1–2), 55–78.
Amorosi, A., Pavesi, M., Ricci Lucchi, M., Sarti, G., Piccin, A., 2008. Climatic signature of cyclic fluvial architecture from the Quaternary of the central Po Plain, Italy. Sediment. Geol. 209, 58–68.
Amorosi, A., Rossi, V., Scarponi, D., Gosh, A., 2014. Biosedimentary record of postglacial coastal dynamics: high-resolution sequence stratigraphy from the northern Tuscan coast (Italy). Boreas 43, 939–954.
Amorosi, A., Bruno, L., Campo, B., Morelli, A., Rossi, V., Scarponi, D., Hong, W., Bohacs, K.M., Drexler, T.M., 2017. Global sea-level control on local parasequence architecture from the Holocene record of the Po Plain, Italy. Mar. Petrol. Geol. 87, 99–111.
Amorosi, A., Barbieri, G., Bruno, L., Campo, B., Drexler, T.M., Hong, W., Rossi, V., Sammartino, I., Scarponi, D., Vaiani, S.C., 2019. Three-fold nature of coastal progradation during the Holocene eustatic highstand, Po Plain, Italy–close correspondence of stratal character with distribution patterns. Sedimentology 66, 3029–3052.
Amorosi, A., Bruno, L., Campo, B., Costagli, B., Dinelli, E., Hong, W., Sammartino, I., Vaiani, S.C., 2020. Tracing clinothem geometry and sediment pathways in the prograding Holocene Po Delta system through integrated core stratigraphy. Basin Res. 32, 206–215.
Amorosi, A., Bruno, L., Campo, B., Costagli, B., Hong, W., Picotti, V., Vaiani, S.C., 2021. Deformation patterns of upper Quaternary strata and their relation to active tectonics, Po Basin, Italy. Sedimentology 68, 402–424. https://doi.org/10.1111/sed.12784.
Athersuch, J., Horne, D.J., Whittaker, J.E., 1989. Marine and brackish water ostracods. In: Kermack, D.M., Barnes, R.S.K. (Eds.), Synopses of the British Fauna. Brill, Leiden/New York/Kopenaghen/Koln, 43.
Auclair, M., Lamothe, M., Huot, S., 2003. Measurement of anomalous fading for feldspar IRSL using SAR. Radiat. Meas. 37, 487–492.
Bacon, M.P., 1984. Glacial to interglacial changes in carbonate and clay sedimentation in the Atlantic Ocean estimated from 230Th measurements. Chem. Geol. 46 (2), 97–111.
Balescu, S., Lamothe, M., 1994. Comparison of TL and IRSL age estimates of feldspar coarse grains from waterlain sediments. Quat. Sci. Rev. 13, 437–444.
Barbieri, G., Vaiani, S.C., 2018. Benthic foraminifera or Ostracoda? Comparing the accuracy of palaeoenvironmental indicators from a Pleistocene lagoon of the Romagna coastal plain (Italy). J. Micropalaeontol. 37, 203–230.
Barbieri, G., Rossi, V., Vaiani, S.C., Dasgupta, U., Amorosi, A., 2021. Quantitative paleoecology in shallow-marine settings: the value of ostracods and foraminifers from the Holocene North Adriatic record. Palaeogeogr. Palaeoclimatol. Palaeoecol. 572, 110408. https://doi.org/10.1016/j.palaeo.2021.110408.
Bentham, P.A., Burbank, D.W., Puigdefàbregas, C., 1992. Temporal and spatial controls on the alluvial architecture of an axial drainage system: late Eocene Escanilla Formation, southern Pyrenean foreland basin, Spain. Basin Res. 4, 335–352. https://doi.org/10.1111/j.1365-2117.1992.tb00052.x.
Beug, H., 2004. Leitfaden der Pollenbestimmung für Mitteleuropa und angrenzende Gebiete. Verlag Dr. Friedrich Pfeil. Verlag Dr. Friederich Pfeil, München, p. 542.
Blum, M.D., 2007. Large River systems and climate change. In: Gupta, A. (Ed.), Large Rivers. https://doi.org/10.1002/9780470723722.ch30.
Blum, M.D., Aslan, A., 2006. Signatures of climate vs. sea-level change within incised valley successions: quaternary examples from the Texas Coastal Plain and Shelf. Sediment. Geol. 190, 177–211.
Blum, M., Martin, J., Milliken, K., Garvin, M., 2013. Paleovalley systems: insights from Quaternary analogs and experiments. Earth Sci. Rev. 116, 128–169.
Boccaletti, M., Corti, G., Martelli, L., 2011. Recent and active tectonics of the external zone of the Northern Apennines (Italy). Int. J. Earth Sci. 100 (6), 1331–1348.
Bonini, L., Toscani, G., Seno, S., 2014. Threedimensional segmentation and different rupture behaviour during the 2012 Emilia seismic sequence (Northern Italy). Tectonophysics 630, 33–42.
Bowen, D.Q., 2010. Sea level~ 400 000 years ago (MIS 11): analogue for present and future sea-level? Clim. Past 6 (1), 19–29.
Bridge, J.S., 1993. The interaction between channel geometry, water flow, sediment transport and deposition in braided rivers. Geological Society, London, Special Publications 75 (1), 13–71.
Bronk Ramsey, C., Lee, S., 2013. Recent and planned developments of the program OxCal. Radiocarbon 55, 720–730.
Bruno, L., Bohacs, K.M., Campo, B., Drexler, T.M., Rossi, V., Sammartino, I., Scarponi, D., Hong, W., Amorosi, A., 2017. Early Holocene transgressive paleogeography in the Po coastal plain (northern Italy). Sedimentology 64 (7), 1792–1816.
Bruno, L., Campo, B., Di Martino, A., Hong, W., Amorosi, A., 2019. Peat layer accumulation and post-burial deformation during the mid-late Holocene in the Po coastal plain (Northern Italy). Basin Res. 31, 621–639. https://doi.org/10.1111/bre.12339.
Bruno, L., Campo, B., Costagli, B., Stouthamer, E., Teatini, P., Zoccarato, C., Amorosi, A., 2020. Factors controlling natural subsidence in the Po Plain. Proceedings of the International Association of Hydrological Sciences 382, 285–290.
Bruno, L., Amorosi, A., Sammartino, I., Lugli, S., Fontana, D., 2021. Trunk river and tributary interactions recorded in the Pleistocene–Holocene stratigraphy of the Po Plain (northern Italy). Sedimentology 68 (6), 2918–2943.
Bruno, L., Campo, B., Hajdas, I., Hong, W., Amorosi, A., 2022. Timing and mechanisms of sediment accumulation and pedogenesis: insights from the Po Plain (northern Italy). Palaeogeogr. Palaeoclimatol. Palaeoecol. 591, 110881.
Buol, S.W., Southard, R.J., Graham, R.C., McDaniel, P.A., 2011. Soil Genesis and Classification. John Wiley & Sons, Chichester, p. 543. https://doi.org/10.1002/9780470960622.
Busschers, F.S., Weerts, H.J.T., Wallinga, J., Cleveringa, P., Kasse, C., De Wolf, H., Cohen, K.M., 2005. Sedimentary architecture and optical dating of Middle and Late Pleistocene Rhine-Meuse deposits-fluvial response to climate change, sea-level fluctuation and glaciation. Neth. J. Geosci. 84 (1), 25–41.
Buylaert, J.P., Murray, A.S., Thomsen, K.J., Jain, M., 2009. Testing the potential of an elevated temperature IRSL signal from K-feldspar. Radiat. Meas. 44, 560–565.
Calabrese, L., Centineo, M.C., Cibin, U., 2008. Note Illustrative Della Carta Geologica d’Italia Alla Scala 1:50.000, Foglio 204 Portomaggiore, p. 98. https://www.isprambiente.gov.it/Media/carg/note_illustrative/204_Portomaggiore.pdf.
Campo, B., Amorosi, A., Vaiani, S.C., 2017. Sequence stratigraphy and late Quaternary paleoenvironmental evolution of the Northern Adriatic coastal plain (Italy). Palaeogeogr. Palaeoclimatol. Palaeoecol. 466, 265–278.
Campo, B., Bruno, L., Amorosi, A., 2020. Basin-scale stratigraphic correlation of late Pleistocene-Holocene (MIS 5e-MIS 1) strata across the rapidly subsiding Po Basin (northern Italy). Quat. Sci. Rev. 237, 106300.
Camuera, J., Jiménez-Moreno, G., Ramos-Román, M.J., García-Alix, A., Toney, J.L., Anderson, R.S., Carrión, J.S., 2019. Vegetation and climate changes during the last two glacial-interglacial cycles in the western Mediterranean: a new long pollen record from Padul (southern Iberian Peninsula). Quat. Sci. Rev. 205, 86–105.
Carminati, E., Doglioni, C., 2012. Alps vs. Apennines: the paradigm of a tectonically asymmetric Earth. Earth Sci. Rev. 112, 67–96.

Carter, R.M., Naish, T.R., 1998. A Review of Wanganui Basin, New Zealand: global reference section for shallow marine, Plio-Pleistocene (2.5–0Ma) Cyclostratigraphy. Sediment. Geol. 122, 37–52.
Catuneanu, O., 2017. Sequence stratigraphy: guidelines for a standard methodology. In: Stratigraphy & Timescales, vol. 2. Elsevier Inc, pp. 1–57. https://doi.org/10.1016/bs.sats.2017.07.003. ISSN 2468-5178.
Changsong, L., Herong, Z., Jianye, R., Jingyan, L., Yigang, Q., 2004. The control of syndepositional faulting on the Eogene sedimentary basin fills of the Dongying and Zhanhua sags, Bohai Bay Basin. Science in China Ser. D Earth Sciences 47 (9), 769–782.
Chaumillon, E., Bertin, X., Falchetto, H., Allard, J., Weber, N., Walker, P., et al., 2008. Multi time-scale evolution of a wide estuary linear sandbank, the Longe de Boyard, on the French Atlantic coast. Mar. Geol. 251 (3–4), 209–223.
Coccioni, R., 2000. Benthic foraminifera as bioindicators of heavy metal pollution – a case study from the Goro Lagoon (Italy). In: Martin, R.E. (Ed.), In Environmental Micropaleontology: the Application of Microfossils to Environmental Geology. Kluwer Academic Publishers/Plenum Press, New York, pp. 71–103.
Collinson, J.D., 1978. Alluvial sediments. In: Reading, H.G. (Ed.), Sedimentary Environments and Facies, second ed., pp. 20–67 (Blackwell, Oxford).
Cui, S., Liu, H., Tong, S., Zhang, J., Wu, Z., Wu, J., 2008. Seismic stratigraphy of the quaternary yellow river delta, bohai sea, eastern China. Marine Geophysical Research 29, 27–42.
Debenay, J.-P., Guillou, J.J., Redois, F., Geslin, E., 2000. Distribution trends of foraminiferal assemblages in paralic environments. A base for using foraminifera as bioindicators. In: Martin, R.E. (Ed.), Environmental Micropaleontology the Application of Microfossils to Environmental Geology. Kluwer Academic/Plenum Publisher, New York, pp. 39–67.
DeCelles, P.G., 2012. Foreland basin systems revisited: variations in response to tectonic settings. In: Busby, C., Azor Pérez, A. (Eds.), Tectonics of Sedimentary Basins: Recent Advances, 2012. Blackwell Publishing Ltd., U.S., pp. 405–426
Demurtas, L., Bruno, L., Lugli, S., Fontana, D., 2022. Evolution of the Po alpine river system during the last 45 Ky inferred from stratigraphic and compositional evidence (ostiglia, northern Italy). Geosciences 12, 342.
Demurtas, L., Fontana, D., Lugli, S., Bruno, L., 2024. Multi-source detrital contributions in the Po alluvial basin (northern Italy) since the Middle Pleistocene. Insights into sediment accumulation in intermediate sinks. Basin Res. 36 (1), e12858.
Di Pasquale, G., Allevato, E., Cocchiararo, A., Moser, D., Pacciarelli, M., Saracino, A., 2014. Late Holocene persistence of Abies alba in low-mid altitude deciduous forests of central and southern Italy: new perspectives from charcoal data. J. Veg. Sci. 25, 1299–1310.
Di Rita, F., Sottili, G., 2019. Pollen analysis and tephrochronology of a MIS 13 lacustrine succession from eastern sabatini volcanic district (rignano flaminio, central Italy). Quat. Sci. Rev. 204, 78–93.
Coal facies and depositional environment. In: Diessel, C.F.K. (Ed.), 1992. Coal-Bearing Depositional Systems. Springer, Berlin, pp. 161–264.
DISS Working Group, 2018. Database of Individual Seismogenic Sources (DISS), Version 3.2.0: A Compilation of Potential Sources for Earthquakes Larger than M 5.5 in Italy and Surrounding Areas. Istituto Nazionale di Geofisica e Vulcanologia. https://doi.org/10.6092/INGV.IT-DISS3.2.0.
Durcan, J., King, G.E., Duller, G.A.T., 2015. DRAC: dose rate and age calculator for trapped charge dating. Quat. Geochronol. 28, 54–61.
Dutton, A., Bard, E., Antonioli, F., Esat, T.M., Lambeck, K., McCulloch, M.T., 2009. Phasing and amplitude of sea-level and climate change during the penultimate interglacial. Nat. Geosci. 2 (5), 355–359.
Dutton, A., Carlson, A.E., Long, A.J., Milne, G.A., Clark, P.U., DeConto, R., et al., 2015. Sea-level rise due to polar ice-sheet mass loss during past warm periods. Science 349 (6244), aaa4019.
Ellis, B.F., Messina, A.R., 1940. Catalogue of Foraminifera. Micropaleontology Press, New York.
Ellis, B.F., Messina, A.R., 1952. Catalogue of ostracoda. American Museum of Natural History Special Publications, New York (Over 23 volumes in loose-leaf form.).
ENEL-DCO, 1984. Localizzazione di un impianto nucleare nella Regione Lombardia, completamento degli studi geologici e geomorfologici locali. Area di Viadana; Area di S. Benedetto Po; Dorsale Ferrarese: Rome, Ente Nazionale per L'Energia Elettrica–Direzione delle Costruzioni, 3 volumes.
Fantoni, R., Franciosi, R., 2010. Tectono-sedimentary setting of the Po Plain and adriatic foreland. Rendiconti Lincei 21, 197–209.
Ferranti, L., Antonioli, F., Mauz, B., Amorosi, A., Dai Pra, G., Mastronuzzi, G., et al., 2006. Markers of the last interglacial sea-level high stand along the coast of Italy: tectonic implications. Quat. Int. 145, 30–54.
Fielding, C.R., 2021. Late Palaeozoic cyclothems – A review of their stratigraphy and sedimentology. Earth-Science Reviews 217, 103612.
Follieri, M., Magri, D., Sadori, L., 1986. Late Pleistocene Zelkova extinction in Central Italy. New Phytol. 103, 269–273.
Follieri, M., Magri, D., Sadori, L., 1988. A 250 000-years pollen record from Valle di Castiglione (Roma). Pollen Spores 30, 329–356.
Fusco, F., Colalongo, M.L., Fiorini, F., 2003. Micropaleontologia e Palinologia del sondaggio profondo 222-S2. In: Calabrese, L., Cibin, U. (Eds.), Note Illustrative Della Carta Geologica d'Italia Alla Scala 1:50.000, Foglio 222 Lugo, Italian. Available online at: https://www.isprambiente.gov.it/Media/carg/note_illustrative/222_Lugo.pdf.
Gao, L., Long, H., Hou, Y., Feng, Y., 2022. Chronology constraints on the complex sedimentary stratigraphy of the paleo-Yangtze incised valley in China. Quat. Sci. Rev. 287, 107573.
Garzanti, E., Vezzoli, G., Andò, S., 2011. Paleogeographic and paleodrainage changes during Pleistocene glaciations (Po plain, northern Italy). Earth Sci. Rev. 105, 25–48.
Ghielmi, M., Minervini, M., Nini, C., Rogledi, S., Rossi, M., 2013. Late Miocene–Middle Pleistocene sequences in the Po Plain–Northern Adriatic Sea (Italy): the stratigraphic record of modification phases affecting a complex foreland basin. Mar. Petrol. Geol. 42, 50–81.
Grant, K.M., Rohling, E.J., Ramsey, C.B., Cheng, H., Edwards, R.L., Florindo, F., et al., 2014. Sea-level variability over five glacial cycles. Nat. Commun. 5 (1), 5076. https://doi.org/10.1038/ncomms6076.
Guérin, G., Mercier, N., Adamiec, G., 2011. Dose-rate conversion factors: update. Ancient TL 29, 5–8.
Gunderson, K.L., Pazzaglia, F.J., Picotti, V., Anastasio, D.A., Kodama, K.P., Rittenou, R. T., Frankel, K.F., Ponza, A., Berti, C., Negri, A., Sabbatini, A., 2014. Unraveling tectonic and climatic controls on synorogenic growth strata (Northern Appennines, Italy). GSA Bulletin 126–3 (4), 532–552.
Hampson, G.J., 2016. Towards a sequence stratigraphic solution set for autogenic processes and allogenic controls: upper Cretaceous strata, Book Cliffs, Utah, USA. J. Geol. Soc. 173, 817–836.
Head, M.J., Gibbard, P.L., 2005. Early-Middle Pleistocene transitions: an overview and recommendation for the defining boundary. Geological Society, London, Special Publications 247 (1), 1–18.
Head, M.J., Gibbard, P.L., 2015. Early–Middle Pleistocene transitions: linking terrestrial and marine realms. Quat. Int. 389, 7–46.
Hearty, P.J., Hollin, J.T., Neumann, A.C., O'Leary, M.J., McCulloch, M., 2007. Global sea-level fluctuations during the Last Interglaciation (MIS 5e). Quat. Sci. Rev. 26 (17–18), 2090–2112.
Henderson, P.A., 1990. Freshwater ostracods. In: Kermack, D.M., Barnes, R.S.K. (Eds.), Synopses of the British Fauna, Universal Book Services. Oegstgeest, The Netherlands. Dr. W. Backhuys.
Henrich, R., Kassens, H., Vogelsang, E., Thiede, J., 1989. Sedimentary facies of glacial-interglacial cycles in the Norwegian Sea during the last 350 ka. Mar. Geol. 86 (4), 283–319.
Hollis, R.J., Wallace, D.J., Miner, M.D., Gal, N.S., Dike, C., Flocks, J.G., 2019. Late Quaternary evolution and stratigraphic framework influence on coastal systems along the north-central Gulf of Mexico, USA. Quat. Sci. Rev. 223, 105910.
Huntley, D.J., Baril, M.R., 1997. The K content of the K-feldspars being measured in optical dating or in the thermoluminescence dating. Ancient TL 15 (1), 11–13.
Huntley, D.J., Hancock, R.G.V., 2001. The Rb contents of the K-feldspar grains being measured in optical dating. Ancient TL 19 (2), 43–46.
Huntley, D.J., Lamothe, M., 2001. Ubiquity of anomalous fading in K-feldspars and the measurement and correction for it in optical dating. Can. J. Earth Sci. 38, 1093–1106.
Jorissen, F., 1988. Benthic foraminifera from the Adriatic Sea; principles of phenotypic variation. Utrecht Micropaleontol. Bull. 176.
Kopp, R.E., Simons, F.J., Mitrovica, J.X., Maloof, A.C., Oppenheimer, M., 2009. Probabilistic assessment of sea level during the last interglacial stage. Nature 462 (7275), 863–867.
Krapez, B., 1996. Sequence stratigraphic concepts applied to the identification of basin-filling rhythms in Precambrian successions. Aust. J. Earth Sci. 43 (4), 355–380.
Larter, R.D., Cunningham, A.P., 1993. The depositional pattern and distribution of glacial-interglacial sequences on the Antarctic Peninsula Pacific margin. Mar. Geol. 109 (3–4), 203–219.
Lea, D.W., Martin, P.A., Pak, D.K., Spero, H.J., 2002. Reconstructing a 350 ky history of sea level using planktonic Mg/Ca and oxygen isotope records from a Cocos Ridge core. Quat. Sci. Rev. 21 (1–3), 283–293.
Lisiecki, L.E., Raymo, M.E., 2005. A Pliocene-Pleistocene stack of 57 globally distributed benthic δ18O records. Paleoceanography 20 (1). https://doi.org/10.1029/2004PA001071PA1003.
Liu, Z., Yin, P., Xiong, Y., Berné, S., Trentesaux, A., Li, C., 2003. Quaternary transgressive and regressive depositional sequences in the East China Sea. Chin. Sci. Bull. 48, 81–87.
Liu, J., Cao, D., Tan, J., Zhang, Y., 2023. Gzhelian cyclothem development in the western North China cratonic basin and its glacioeustatic, tectonic, climatic and autogenic implications. Mar. Petrol. Geol., 106355 https://doi.org/10.1016/j.marpetgeo.2023.106355.
Loutre, M.F., Berger, A., 2003. Marine Isotope Stage 11 as an analogue for the present interglacial. Global Planet. Change 36 (3), 209–217.
Magri, D., 1999. Late Quaternary vegetation history at Lagaccione near Lago di Bolsena (central Italy). Rev. Palaeobot. Palynol. 106, 171–208.
Magri, D., Di Rita, F., 2015. Archaeopalynological preparation techniques. In: Yeung, E. C.T., Stasolla, C., Sumner, M.J., Huang, B.Q. (Eds.), Plant Microtechniques and Protocols. Springer International Publishing, Cham, pp. 495–506.
Magri, D., Agrillo, E., Di Rita, F., Furlanetto, G., Pini, R., Ravazzi, C., Spada, F., 2015. Holocene dynamics of tree taxa populations in Italy. Rev. Palaeobot. Palynol. 218, 267–284.
Magri, D., Di Rita, F., Aranbarri, J., Fletcher, W., González-Sampériz, P., 2017. Quaternary disappearance of tree taxa from Southern Europe: timing and trends. Quat. Sci. Rev. 163, 23–55.
Marcolla, A., Miola, A., Mozzi, P., Monegato, G., Asioli, A., Pini, R., Stefani, C., 2021. Middle Pleistocene to Holocene palaeoenvironmental evolution of the south-eastern Alpine foreland basin from multi-proxy analysis. Quat. Sci. Rev. 259, 106908. https://doi.org/10.1016/j.quascirev.2021.106908.
Marković, S.B., Oches, E.A., McCoy, W.D., Gaudenyi, T., Frechen, M., 2007. Malacological and sedimentological evidence for "warm" glacial climate from the Irig loess sequence, Vojvodina, Serbia. Geochem. Geophys. Geosyst. 8, Q09008. https://doi.org/10.1029/2006GC001565.
Marks, L., Bińka, K., Woronko, B., Majecka, A., Teodorski, A., 2019. Revision of the late Middle Pleistocene stratigraphy and palaeoclimate in Poland. Quat. Int. 534, 5–17.

Massari, F., Rio, D., Barbero, R.S., Asioli, A., Capraro, L., Fornaciari, E., Vergerio, P.P., 2004. The environment of Venice area in the past two million years. Palaeogeogr. Palaeoclimatol. Palaeoecol. 202 (3–4), 273–308.
Meisch, C., 2000. In: Schwoerbel, J., Zwick, P. (Eds.), Freshwater Ostracoda of Western and Central Europe. Süsswasserfauna von Mitteleuropa 8/3. Spektrum Akademischer Verlag, Heidelberg, Berlin, p. 522.
Mejdahl, V., 1979. Thermoluminescence dating: beta-dose attenuation in quartz grains. Archaeometry 21, 61–72.
Miall, A.D., 1985. Architectural-element analysis: a new method of facies analysis applied to fluvial deposits. Earth Sci. Rev. 22 (4), 261–308.
Miall, A.D., 1996. The geology of fluvial deposits: sedimentary facies. In: Basin Analysis, and Petroleum Geology. Springer-Verlag, Berlin, p. 582.
Murray, J.W., 2006. Ecology and Applications of Benthic Foraminifera. Cambridge University Press, Cambridge, p. 426.
Muttoni, G., Carcano, C., Garzanti, E., Ghielmi, M., Piccin, A., Pini, R., Rogledi, S., Sciunnach, D., 2003. Onset of major Pleistocene glaciations in the Alps. Geology 31, 989–992. https://doi.org/10.1130/G19445.1.
Muttoni, G., Scardia, G., Kent, D.V., Morsiani, E., Tremolada, F., Cremaschi, M., Peretto, C., 2011. First dated human occupation of Italy at ~0.85 Ma during the late Early Pleistocene climate transition. Earth Planet Sci. Lett. 307, 241–252. https://doi.org/10.1016/j.epsl.2011.05.025.
Nielsen, K.A., Clemmensen, L.B., Fornós, J.J., 2004. Middle Pleistocene magnetostratigraphy and susceptibility stratigraphy: data froma carbonate aeolian system, Mallorca, Western Mediterranean. Quat. Sci. Rev. 23, 1733–1756.
Non-Pollen Palynomoprh Image Database. https://non-pollen-palynomorphs.uni-goettingen.de. Accessed 13 July 2023.
Obreht, I., Zeeden, C., Hambach, U., Veres, D., Marković, S.B., Bösken, J., Svirčev, Z., Bačević, N., Gavrilov, M.B., Lehmkuhl, F., 2016. Tracing the influence of Mediterranean climate on Southeastern Europe during the past 350,000 years. Sci. Rep. 6, 36334.
Orain, R., Lebreton, V., Ermolli, E.R., Combourieu-Nebout, N., Sémah, A.M., 2013. Carya as marker for tree refuges in southern Italy (Boiano basin) at the Middle Pleistocene. Palaeogeogr. Palaeoclimatol. Palaeoecol. 369, 295–302.
Ori, G.G., 1993. Continental depositional systems of the Quaternary of the Po Plain (northern Italy). Sediment. Geol. 83, 1–14.
PalDat-Palynological Database. https://www.paldat.org. Accessed Oct 2023.
Peeters, J., Busschers, F.S., Stouthamer, E., Bosch, J.H.A., Van den Berg, M.W., Wallinga, J., et al., 2016. Sedimentary architecture and chronostratigraphy of a late Quaternary incised-valley fill: a case study of the late Middle and Late Pleistocene Rhine system in The Netherlands. Quat. Sci. Rev. 131, 211–236.
Pini, R., Ravazzi, C., Donegana, M., 2009. Pollen stratigraphy, vegetation and climate history of the last 215ka in the Azzano Decimo core (plain of Friuli, north-eastern Italy). Quat. Sci. Rev. 28, 1268–1290.
Pini, R., Ravazzi, C., Reimer, P.J., 2010. The vegetation and climate history of the last glacial cycle in a new pollen record from Lake Fimon (southern Alpine foreland, N-Italy). Quat. Sci. Rev. 29, 3115–3137.
Prescott, J.R., Hutton, J.T., 1994. Cosmic ray contributions to dose rates for luminescence and ESR dating. Radiat. Meas. 23, 497–500.
Raymo, M.E., Mitrovica, J.X., 2012. Collapse of polar ice sheets during the stage 11 interglacial. Nature 483 (7390), 453–456.
Reille, M., 1992. Pollen et spores d'Europe et d'Afrique du Nord. Laboratoire De Botanique Historique Et Palynologie, Marseille, p. 543.
Reimer, P.J., Austin, W.E., Bard, E., Bayliss, A., Blackwell, P.G., Ramsey, C.B., et al., 2020. The IntCal20 Northern Hemisphere radiocarbon age calibration curve (0–55 cal kBP). Radiocarbon 62 (4), 725–757.
Ricci Lucchi, F., Colalongo, M.L., Cremonini, G., Gasperi, G., Iaccarino, S., Papani, G., Raffi, S., Rio, D., 1982. Evoluzione sedimentaria e paleogeografica nel margine appenninico. In: Cremonini, G., Ricci Lucchi, F. (Eds.), Guida alla Geologia del Margine Appenninico-Padano. *Guida Geol. Reg., Soc.* Geol. It., pp. 17–46
Richardson, J.L., Vepraskas, M.J., 2001. Wetland Soilsgenesis, Hydrology, Landscapes, and Classification. CRC Press, LLC, Boca Raton, FL, p. 417.
Rohling, E.J., Grant, K., Bolshaw, M., Roberts, A.P., Siddall, M., Hemleben, C., Kucera, M., 2009. Antarctic temperature and global sea level closely coupled over the past five glacial cycles. Nat. Geosci. 2 (7), 500–504.
Rohling, E.J., Grant, K.M., Roberts, A.P., Larrasoana, J.C., 2013. Paleoclimate variability in the Mediterranean and Red Sea regions during the last 500,000 years: implications for hominin migrations. Curr. Anthropol. 54 (S8), S183–S201.
Rohling, E.J., Foster, G.L., Grant, K.M., Marino, G., Roberts, A.P., Tamisiea, M.E., Williams, F., 2014. Sea-level and deep-sea-temperature variability over the past 5.3 million years. Nature 508 (7497), 477–482.
Rose, J., 2009. Early and middle Pleistocene landscapes of eastern england. Proc. Geologists' Assoc. 120 (1), 3–33.
Rossi, V., Amorosi, A., Sarti, G., Mariotti, S., 2017. Late Quaternary multiple incised-valley systems: an unusually well-preserved stratigraphic record of two interglacial valley-fill successions from the Arno Plain (northern Tuscany, Italy). Sedimentology 64, 1901–1928.
Rossi, V., Amorosi, A., Barbieri, G., Vaiani, S.C., Germano, M., Campo, B., 2021. A long-term record of quaternary facies patterns and palaeonvironmental trends from the Po plain (NE Italy) as revealed by bio-sedimentary data. Geosciences 11 (10), 401.
Rovere, A., Vacchi, M., Firpo, M., Carobene, L., 2011. Underwater geomorphology of the rocky coastal tracts between finale ligure and vado ligure (western liguria, NW mediterranean sea). Quat. Int. 232 (1–2), 187–200.
Rovere, A., Raymo, M.E., Vacchi, M., Lorscheid, T., Stocchi, P., Gomez-Pujol, L., et al., 2016. The analysis of Last Interglacial (MIS 5e) relative sea-level indicators: Reconstructing sea-level in a warmer world. Earth Sci. Rev. 159, 404–427.
Russo Ermolli, E., 1994. Analyse pollinique de la succession lacustre pléistocène du Vallo di Diano (Campanie, Italie). Ann. Soc. Geol. Belg. 117, 333–354.
Scarponi, D., Kowalewski, M., 2007. Sequence stratigraphic anatomy of diversity patterns: late Quaternary benthic mollusks of the Po Plain, Italy. Palaios 22 (3), 296–305.
Scarponi, D., Huntley, J.W., Capraro, L., Raffi, S., 2014. Stratigraphic paleoecology of the Valle di Manche section (Crotone Basin, Italy): a candidate GSSP of the Middle Pleistocene. Palaeogeogr. Palaeoclimatol. Palaeoecol. 402, 30–43.
Serandei Barbero, R., Albani, A., Bonardi, M., 2004. Ancient and modern salt marshes in the Lagoon of Venice. Palaeogeogr. Palaeoclimatol. Palaeoecol. 202, 229–244.
Siddall, M., Chappell, J., Potter, E.K., 2007. 7. Eustatic sea level during past interglacials. In: Developments in Quaternary Sciences, vol. 7. Elsevier, pp. 75–92.
Stolt, M.H., Rabenhorst, M.C., 2011. Introduction and historical development of subaqueous soil concepts. In: Huang, P.M., Li, Y., Sumner, M.L. (Eds.), Handbook of Soil Sciences Properties and Processes. CRC Press, LLC, Boca Raton, FL. https://www.routledgehandbooks.com/doi/10.1201/b11267-71.
Storms, J.E., Weltje, G.J., Terra, G.J., Cattaneo, A., Trincardi, F., 2008. Coastal dynamics under conditions of rapid sea-level rise: late Pleistocene to Early Holocene evolution of barrier–lagoon systems on the northern Adriatic shelf (Italy). Quat. Sci. Rev. 27 (11–12), 1107–1123. https://doi.org/10.1016/j.quascirev.2008.02.009.
Sun, J., Guo, F., Wu, H., Yang, H., Qiang, X., Chu, H., He, L., Mei, X., Jiang, J., Wang, S., Liu, J., Chen, X., 2022. The sedimentary succession of the last 2.25 Myr in the Bohai Strait: Implications for the Quaternary paleoenvironmental evolution of the Bohai Sea. Palaeogeogr., Palaeoclimatol., Palaeoecol. 585, 1–12.
Swift, D.J.P., 1968. Coastal erosion and transgressive stratigraphy. J. Geol. 76, 444–456.
Tanabe, S., Nakanishi, T., Ishihara, Y., Nakashima, R., 2015. Millennial-scale stratigraphy of a tide-dominated incised valley during the last 14 kyr: spatial and quantitative reconstruction in the Tokyo Lowland, central Japan. Sedimentology 62 (7), 1837–1872. https://doi:10.1111/sed.12204.
Tentori, D., Mancini, M., Milli, S., Stigliano, F., Tancredi, S., Moscatelli, M., 2022. Compositional, micromorphological and geotechnical characterization of Holocene Tiber floodplain deposits (Rome, Italy) and sequence stratigraphic implications. Sedimentology 69 (4), 1705–1737. https://doi.org/10.1111/sed.12969.
Thanh, N.T., Cuong, D.H., Stattegger, K., Dung, B.V., Yang, S., Chi, N.T.K., Tung, N.X., Tinh, N.V., Nga, N.T., 2021. Depositional sequences of the Mekong river delta and adjacent shelf over the past 140 kyr, southern Vietnam. J. Asian Earth Sci. 206, 104634.
The Global Pollen Project. https://globalpollenproject.org. Accessed Oct 2023.
Thomsen, K.J., Murray, A.S., Jain, M., Bøtter-Jensen, L., 2008. Laboratory fading rates of various luminescence signals from feldspar-rich sediment extracts. Radiat. Meas. 43, 1474–1486.
Thomson, J., Nixon, S., Summerhayes, C.P., Schönfeld, J., Zahn, R., Grootes, P., 1999. Implications for sedimentation changes on the Iberian margin over the last two glacial/interglacial transitions from (230Thexcess) 0 systematics. Earth Planet Sci. Lett. 165 (3–4), 255–270.
Toscani, G., Burrato, P., Di Bucci, D., Seno, S., Valensise, G., 2009. Plio-Quaternary tectonic evolution of the Northern Apennines thrust fronts (Bologna-Ferrara section, Italy): seismotectonic implications. Italian Journal of Geosciences 128 (2), 605–613.
Tropeano, M., Sabato, L., Pieri, P., 2002. Filling and cannibalization of a foredeep: the Bradanic Trough, southern Italy. In: Geological Society, vol. 191. Spec. Publ., London, pp. 55–79.
Turrini, C., Lacombe, O., Roure, F., 2014. Present-day 3D structural model of the Po Valley basin, Northern Italy. Mar. Petrol. Geol. 56, 266–289.
Tzedakis, P.C., Andrieu, V., de Beaulieu, J.-L., Crowhurst, S., Follieri, M., Hooghiemstra, H., Magri, D., Reille, M., Sadori, L., Shackleton, N., Wijmstra, T.A., 1997. Comparison of terrestrial and marine record of changing climate of the last 500,000 years. Earth Planet Sci. Lett. 50, 171–176.
Vis, G.J., Kasse, C., 2009. Late quaternary valley-fill succession of the lower tagus valley, Portugal. Sediment. Geol. 221 (1–4), 19–39.
Waelbroeck, C., Labeyrie, L., Michel, E., Duplessy, J.C., Mcmanus, J.F., Lambeck, K., et al., 2002. Sea-level and deep water temperature changes derived from benthic foraminifera isotopic records. Quat. Sci. Rev. 21 (1–3), 295–305.
Wick, L., Möhl, A., 2006. The mid-Holocene extinction of silver fir (Abies alba) in the Southern Alps: a consequence of forest fires? Palaeobotanical records and forest simulations. Veg. Hist. Archaeobotany 15, 435–444.
Xu, T., Wang, G., Shi, X., Wang, X., Yao, Z., Yang, G., et al., 2016. Sequence stratigraphy of the subaqueous changjiang (yangtze river) delta since the last glacial maximum. Sediment. Geol. 331, 132–147.
Yang, Y., 2011. Tectonically-driven underfilled–overfilled cycles, the middle Cretaceous in the northern Cordilleran foreland basin. Sediment. Geol. 233, 15–27.
Yao, Z., Shi, X., Liu, Y., Kandasamy, S., Qiao, S., Li, X., et al., 2020. Sea-level and climate signatures recorded in orbitally-forced continental margin deposits over the last 1 Myr: new perspectives from the Bohai Sea. Palaeogeogr. Palaeoclimatol. Palaeoecol. 550, 109736.
Zazo, C., Goy, J.L., Dabrio, C.J., Lario, J., González-Delgado, J.A., Bardají, T., et al., 2013. Retracing the Quaternary history of sea-level changes in the Spanish Mediterranean–Atlantic coasts: geomorphological and sedimentological approach. Geomorphology 196, 36–49.
Zhang, J., Wan, S., Clift, P.D., Huang, J., Yu, Z., Zhang, K., et al., 2019. History of yellow River and yangtze river delivering sediment to the yellow sea since 3.5 Ma: tectonic or climate forcing? Quat. Sci. Rev. 216, 74–88.